Project ID: 24266

Microneedle Reservoir System for Delivery of Cells to Thick Tissue Scaffolds

A Major Qualifying Report submitted to the faculty of WORCESTER POLYTECHNIC INSTITUTE in partial fulfillment of the requirements for the degree of Bachelor of Science

Submitted by:

Marissa Langille

Keri McLaughlin

Jessica Netto

Julia Ormerod

April 28, 2022

Professor Sakthikumar Ambady, Ph.D., Advisor
Department of Biomedical Engineering

Table of Contents

Table of Figures

Table of Tables

Authorship

This report is the combined effort of Marissa Langille, Keri McLaughlin, Jessica Netto, and Julia Ormerod. Every group member drafted and edited each chapter and section of this report.

Acknowledgments

We would like to thank the following individuals and groups for their involvement in this project:

Professor Sakthikumar Ambady
Ian Anderson
Nancy Burnham
Professor Jeannine Coburn
James Eakin
Rob Kirch
Doug Leonardi
James Loiselle
Jyotsna Patel
Erica Stults
Lisa Wall
Professor Catherine Whittington
User Friendly Characterization Lab

Abstract

Deep tissue injuries, such as severe burns and volumetric muscle loss result in significant function loss from inadequate tissue regeneration. Current treatment options are not optimal. There is a need for a device to recellularize thick tissue scaffolds to promote tissue regeneration in large tissue injuries. This project was aimed at developing a micro/nanoneedle system capable of delivering precise volumes of cell suspension to decellularized tissue scaffolds at least one centimeter thick. The final device consists of two parts: 30g needles and a cell suspension reservoir attached to a motor-driven syringe pump. Verification and validation testing showed that the device can efficiently deliver cell suspension to decellularized tissue up to one centimeter deep.

CHAPTER 1: INTRODUCTION

Volumetric muscle loss (VML) and burn injuries result in large scale muscle injuries incapable of performing natural tissue regeneration. VML is extremely prevalent with military service personnel suffering from a large number of severe trauma incidents classified as volumetric muscle loss injuries. Burn injuries are a common injury experienced among society, with 11 million burn injuries occurring each year. Current treatments for these two pathologies include a variety of different tissue grafts ranging from autografts, allografts, bioengineered skin substitutes, and xenografts. These tissue grafts differ based on the sourcing of the tissue, with autografts using tissue directly sourced from the patient, allografts utilizing tissue from cadavers or a separate patient, and xenografts sourcing tissue from an animal. These treatment options pose risks such as transplant rejection and donor site morbidity; therefore, an alternative is needed.

Decellularized tissue patches could offer scaffolding for thick tissue regeneration, but the process of natural repopulation within the body is not practical time-wise. Microneedles could be useful in delivering large numbers of cells, preferably patient-specific cells, to repopulate the scaffold *in vitro* and subsequent transplantation. Microneedles currently on the market are capable of regenerating tissue at the epidermal level due to their needles only reaching a maximum length of a couple hundred micrometers. Based on this gap in the market, our project aims to develop a microneedle capable of recellularizing one centimeter thick tissue patches, with the goal of using the device to deliver cells to decellularized tissue and observe the viability of the cells.

Throughout the design process, the team followed four main design objectives for our device. These include being capable of delivering cells to tissue patches at least one centimeter thick, incorporating a reservoir for storage of cells prior to injection, preserving the viability of cells during storage and delivery, and being effective for various tissue scaffolds. Many iterations of prototyping were performed to achieve the final design. Once this design was selected, different tests were conducted to analyze the performance of the device.

To test the ability of the device to recellularize tissue, the team optimized a decellularization protocol to remove the cells from bovine skeletal muscle tissue. This decellularized tissue was used to test the ability of our device to repopulate the scaffolds with cells. Three different decellularization protocols were performed to determine the most effective based on the ability to fully remove cells and other cellular components while keeping the extracellular matrix and structure of the tissue intact. Hematoxylin and Eosin (H&E) staining was performed to visualize the presence of cells following decellularization. The most effective protocol was capable of removing all nuclei from the tissue samples and also maintained the integrity of the extracellular matrix (ECM) of the sample. The stability of the ECM was determined through two additional tests on the decellularized tissue (a) Picrosirius Red/Fast Green staining to determine whether the protocol maintained the matrix structure and (b) scanning electron microscopy. Testing was also performed to verify that the scaffolds could

support viable cells after decellularization, as well as after long term storage at -20℃, -80℃, and in liquid nitrogen.

Once the final device was fabricated and a decellularization protocol was finalized, testing was performed to validate the performance of the microneedle device. Leak testing was conducted by submerging the device underwater and passing air through the assembly to ensure air was not released from anywhere other than the needle tips. Flow rate and cell retention were simultaneously tested by delivering cells to one centimeter thick decellularized bovine skeletal muscle with the device as a delivery mechanism. Three different flow rates were tested to determine which allowed for the highest cell retention. This was assessed by performing histology on the tissue samples and visually inspecting for which samples contained cells following delivery, as well as counting the cells in the leaked media following delivery.

CHAPTER 2: LITERATURE REVIEW

2.1 Pathophysiology and Epidemiology

2.1.1 Burn Pathophysiology and Epidemiology

Skin is the largest organ, spanning approximately 1.5-2 square meters [1]. The outer, epidermal layer of skin acts as a protective barrier, a sensory organ in the nervous system, and a mechanism for fluid retention. The inner two layers, the dermis and the hypodermis, regulate temperature, protect the body during trauma, help with epidermal repair, and prevent fluid loss [1], [2]. The skin also contributes to Vitamin D production [1].

Burn injuries interrupt the skin's essential bodily functions, leading to heat loss, infection, water loss, and numbness or paralysis [2]. According to the World Health Organization, 11 million burn injuries occur each year, with 180,000 of these injuries being fatal. The depth and area of the burn injury indicate the severity of the injury [3]. Severe burns cover more than 20% of body surface area in adults [1]. Burn depth can be described by five classifications, as shown in Figure 2.1.

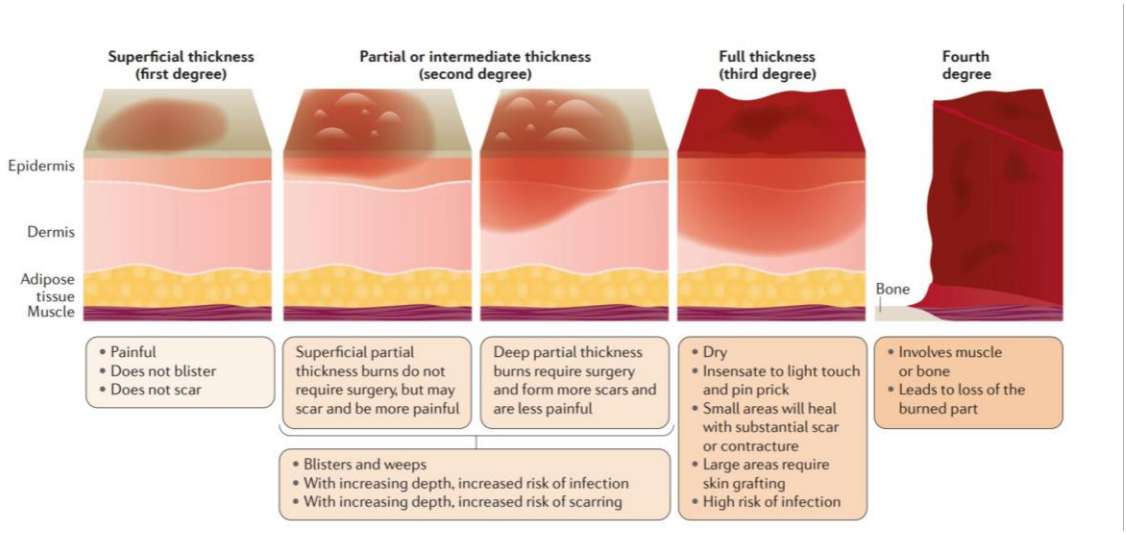

Figure 2.1: Classifications of Burn Depth. The severity of a burn injury depends upon the depth the injury penetrates through the skin. Burn depth is an important factor in patient response and course of treatment [3].

The biological response to a burn injury depends upon the severity, cause, inhalation injury, toxin exposure, and factors related to the patient, such as age [3]. There can be both local and systemic bodily responses following a burn. Local responses divide into three zones: coagulation, stasis or ischemia, and hyperemia. The zone of coagulation is the innermost zone containing the most damage. The stasis zone, or ischemia, is characterized by decreased blood flow and potentially recoverable tissue. The outermost hyperemia zone has increased blood flow, and the tissue should recover if a severe infection does not occur [3], [4]. Severe burns cause a systematic response in the body, which releases cytokines and inflammatory mediators. This systematic response impacts respiratory, cardiovascular, immunological, and metabolic function

[4]. Specifically, the heart, lungs, kidneys, liver, gastrointestinal tract, bone marrow, and the immune system are affected [1], [5]. Burn responses can last for up to 5-10 years after the initial injury [3].

Burn wounds heal in four phases: hemostasis, inflammation, remodeling, and proliferation [3]. Immediately following the injury, hemostasis occurs. Hemostasis causes vasoconstriction, activation of platelets, and release of growth and clotting factors. A fibrin clot also forms at the injury site. Following hemostasis, inflammation occurs and can last for months. During the inflammation phase, monocytes and neutrophils release growth factors, cytokines, and chemokines. Removal of pathogens also occurs. In the third stage, proliferation, extracellular matrix deposition, angiogenesis, and epithelialization occur. During the final remodeling stage, matrix remodeling occurs [3].

2.1.2 Large Volume Muscle Injury Pathophysiology and Epidemiology

Skeletal muscle is the most abundant type of muscle, accounting for 40% of body mass [6], [7]. This type of muscle contains cells known as muscle fibers that receive neural inputs that allow conscious control of them by the brain. These fibers are covered by the sarcolemma, forming transverse tubules that facilitate ion exchange. The endomysium, a connective tissue containing capillaries, covers the sarcolemma. These muscle fibers join together, forming fascicles. The encasing connective tissue around the fascicles is called the perimysium. Together, the fascicles form a structure surrounded by the epimysium, as seen in Figure 2.2. Skeletal muscle is striated due to the composition of actin and myosin filaments that make up the myofibrils [8]. Skeletal muscle facilitates bodily movement via contraction and relaxation. Additionally, skeletal muscle supports body posture, regulates temperature, and plays a role in breathing and swallowing [6], [8]. The force that facilitates this movement is generated by actin and myosin filaments sliding past one another [9].

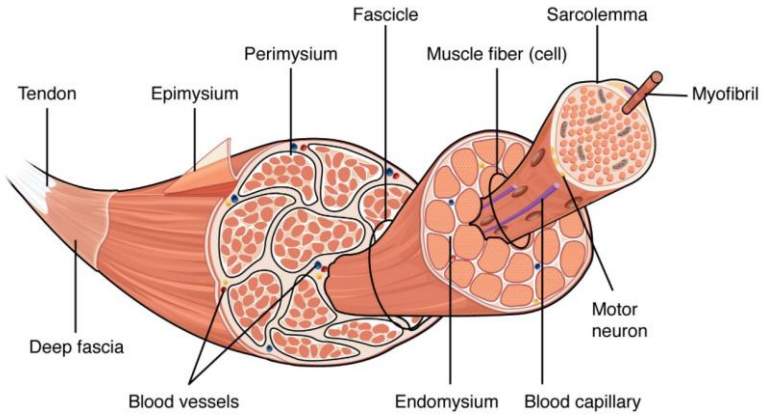

Figure 2.2: The Connective Tissue Layers. These layers come together to form skeletal muscle [9].

Severe, or volumetric, muscle loss occurs when greater than 20% of muscle tissue is lost. With this percentage of muscle loss, the body is incapable of adequate tissue regeneration because skeletal muscle fibers cannot divide, leading to issues such as scarring, fibrosis, and loss of function [6], [7], [10]. Traumas, hereditary defects, vascular deficits, tumor resections, and infections can lead to volumetric muscle loss (VML) [10]. VML most often occurs from combat injuries [6]. Additionally, data on civilian traumas do not identify VML injuries specifically. However, approximately 58% of severe open tibial fractures resulting from trauma are associated with severe muscle injuries [11]. In military populations studied from Operation Enduring Freedom and Operation Iraqi freedom, 65% of service members diagnosed with orthopedic traumas experienced VML [12]. In another study of 14,500 military service members, 8% of the participants received a VML disability rating [13].

Non-VML injuries to skeletal muscle require three stages of repair: the inflammatory stage, the repair stage, and the remodeling stage [6]. During the inflammatory stage, or the destruction stage, myofibril and surrounding tissue damage occur through necrosis. Neutrophils migrate to the injury site to remove debris and damaged cells, as well as promote vascularization. Macrophages also migrate to the injury following neutrophil migration and perform phagocytosis on any necrotic tissue that is left. The macrophages also promote stem cell survival and proliferation. The macrophages switch from inflammatory to anti-inflammatory phenotypes to prompt myoblast proliferation [6]. Following the inflammatory phase, satellite cells in the repair phase help form new muscle cells, and stem cells turn into myoblasts. These myoblasts then cluster to create muscle fibers. During this stage, the fibroblast also generates connective tissue. Blood vessel and nerve generation also occur during the repair phase. The final remodeling phase is when the extracellular matrix forms and the basal lamina acts as a template for myofiber and neuromuscular junction growth. Innervation and vascularization of the injured site also occur [6]. When VML occurs, the typical three stage healing process cannot happen. During VML, the satellite cells and basal lamina are destroyed or removed; therefore, the muscle is difficult to repair [6]. The inability to heal naturally can result in disability, chronic pain, impairment of muscle function, scarring, and cosmetic defects [10].

Patients who have experienced VML have further health considerations. VML patients experience impaired mobility and alterations in muscle fiber phenotype [7], [14]. Current treatments for patients who have experienced VML include surgeries, physical therapy, biological scaffolds, and cell therapies, such as stem cell treatment. The standard surgical treatment is an autologous transplant [6].

2.2 Current Tissue Injury Treatments

Autologous tissue grafts, or tissue autografts, are the gold standard for those with tissue injuries and diseases [15]. Autografts use tissue directly from the patient. Current autograft products on the market include cultured epidermal autografts (CEAs), such as Epicel, a product that treats burn injuries covering 30% of the body's surface area [2], [16]. Epicel, created by Vericel, is an autograft obtained from two biopsies of the patient's healthy skin. A singular

Epicel can cover 7,200 square centimeters in treatment [16]. Autografts are favorable because there is a low risk of disease transmission and rejection, and there is potential for new tissue growth [17]. However, some disadvantages of autografts include donor site morbidity, limited availability, and higher failure rates [15]. These morbidities include pain, infections, and numbness. Autografts also require two surgical procedures, increasing the surgical materials needed and the time a patient stays in the hospital [17]. Autografts are also limited in treating patients with larger wound areas due to a lack of donor tissue area remaining [5].

Another tissue graft used to treat tissue injuries is allogeneic tissue grafts or tissue allografts. Tissue allografts are derived from cadavers or a different patient through surgery [15]. Dermagraft consists of fibroblasts, extracellular matrix (ECM), and an absorbable scaffold [18]. These products are limited to treating only the dermal layer of tissue, making it insufficient for treatment of other tissue injuries such as muscle. Some advantages of allografts include only requiring one additional surgical procedure and eliminating donor site issues, such as infections. This means less time spent in the hospital [17]. However, a disadvantage of allografts is the potential to elicit an immune system reaction and transmit disease. Allograft tissue is also incorporated into the body more slowly than a patient's own tissue [17]. A lack of compatible donors also limits the availability of tissue to use in allografts [19].

Bioengineered skin substitutes can also be used to treat tissue injuries. These skin substitutes are derived from cells cultured in a lab. For example, Apligraf and Dermagraft, from Osteogenesis, are examples of allogeneic grafts that act like skin or dermal substitutes. Apligraf technology contains an epidermal layer with keratinocytes and stem cells to signal healing, as well as a dermal layer containing fibroblasts that produce ECM proteins [20].

Xenogeneic tissue grafts, also known as xenografts, are a third method to repair tissue injury. Xenografts come from animals, with the more common xenografts being bovine and porcine [2], [15]. Integra's Dermal Regeneration Template is an example of a xenogeneic skin graft. The template contains an outer silicon layer and an inner matrix made of bovine collagen and glycosaminoglycan from sharks. The product is beneficial for patients whose tissue is too thin to harvest or who have limited donor sites available. However, this technology has limitations when reconstructing more complicated tissue, such as bones and muscles [21]. Additionally, xenografts could potentially elicit an immune response and contain biological contaminants [15].

Another technology for tissue repair includes a patented viable tissue repair implant. The implant contains a slice of tissue that is a source of viable cells for tissue repair and regeneration. A bioactive agent can be added to the implant to further promote tissue regeneration [22]. The viable cells within the implant migrate and proliferate into the injury site for healing. The patent describes a variety of repairs that this implant could facilitate for various applications such as cosmetic treatments, therapeutic treatments, and tissue remodeling [22]. However, with this product, the implant is fastened to the surrounding tissue with staples, sutures, adhesives, tacks, and fasteners, which introduce synthetic components into the body [22]. Additionally, this product is limited to tissue thicknesses less than 1 mm [22].

Decellularized tissue scaffolds derived from the target tissue of the patient are the optimal scaffold option. However, these scaffolds can also come from allogeneic or xenogeneic materials previously described [15]. These scaffolds allow the seeding of any cell type while preserving the ECM structure [23]. Decellularized scaffolds with autologous cells can decrease a patient's immune response, making them an optimal choice compared to other prior art [19].

2.3 Decellularized Tissue Scaffolds

The field of tissue engineering and regenerative medicine uses biological and artificial materials to maintain, restore, and functionalize tissue [15], [23]. Many of the materials used for artificial scaffolds do not support bioactivity or recapitulate the properties of the extracellular matrix (ECM) [15]. Decellularized tissue scaffolds are a promising material for use in tissue engineering [23]. The decellularization process leads to cell-free, gene-free, and natural ECM that retain their architectural and mechanical properties [15], [24]. The main three methods of decellularization are physical, chemical, or biological methods. Physical methods include freeze-thawing to disrupt the cell membranes. Detergents are commonly used in chemical decellularization. Biological decellularization includes the use of enzymes, specifically nucleases and proteases to degrade DNA, RNA, and proteins. These methods all pose the risk of damaging or altering the ECM and the decellularization methods used should be based on the type of tissue and the use of the ECM [23].

The ECM is present in all human and animal tissue and organs to provide physical support to cells and biochemical, biophysical, and biomechanical signals to the tissue [19], [23]. The signals produced by the ECM lead to morphogenesis, where the tissue develops a shape, differentiation, and homeostasis of the tissue [19]. The ECM is relevant for cell attachment, proliferation, differentiation, and regeneration [24]. A multitude of proteins make up and functionalize the ECM and this make-up is dependent on the tissue it is a part of [23]. The most important ECM proteins are collagens, elastins, proteoglycans, and glycoproteins [23].

Currently, decellularized tissue scaffolds are used to treat injuries to tissue and disease [24]. They are a treatment alternative to organ or tissue transplantation, in which there is a large discrepancy between the number of patients who need an organ and the number that receive an organ [23]. The decellularized scaffolds can be left bare allowing the patient's cells to repopulate the scaffold and replace the decellularized scaffold with new ECM. The scaffolds can also be repopulated before implantation with the patient's own cells which deposit new ECM in the scaffold and proliferate to form new tissue [19].

2.3.1 Recellularization of Decellularized Tissue Scaffolds

Decellularized tissue scaffolds have the potential to be recellularized *in vitro* prior to transplantation or *in vivo* after transplantation. Many cell types can be used to reseed the decellularized scaffold including cell lines, primary cells, mesenchymal stem cells, embryonic stem cells, induced pluripotent stem cells, and engineered stem cells [24]. These cell types offer a range of advantages and disadvantages that need to be considered before choosing a cell type

[19]. For example, cell lines are easy to expand but they are limited in their ability to differentiate. In comparison, many stem cells are easy to expand and have a larger differentiation potential, but there is the risk of tumorigenesis [24]. Mesenchymal and pluripotent stem cells are the most promising for use in decellularized scaffolds because of their ability to differentiate into different cell types, as well as their availability [15], [19]. Recellularization can functionalize the scaffold as if it were a transplanted tissue or organ. This functionality is dependent on cell type as well [24].

2.3.2 Advantages and Limitations of Decellularized Tissue Scaffolds for Wound Healing

Decellularized scaffolds offer advantages in terms of their structure, biological function, and ability to be further modified [23]. The highly detailed architecture of the ECM is preserved in decellularized tissue scaffolds, which is essential for tissue function that relies on the form. These scaffolds can also be scaled to the desired size for a specific application. For example, the choice can be made between a small-scale scaffold derived from a mouse or a larger scaffold derived from a pig. Decellularized tissue scaffolds contain the appropriate ligands for cell signaling that support cell engraftment and survival. This is important for the recellularization of the scaffolds. Cells can also remodel the scaffolds which allow the scaffold to repair itself and adapt over time [23]. Additionally, decellularized tissue scaffolds are highly similar to the tissue being replaced. A patient's own cells can be used in the recellularization process for a patient-specific therapy with a diminished immune response [19]. Finally, decellularized tissue scaffolds can be modified *in vivo* or *ex vivo* if adaptations are needed [23].

The current limitations of decellularized tissue scaffolds include the decellularization process, immunogenicity, and recellularization [24]. The decellularization process is variable due to its specificity to each tissue type. This process should be optimized to improve reproducibility, effectively remove cells, and maintain the integrity of the ECM [23], [24]. However, another limitation of the decellularization process is that the ECM will always be damaged to a certain extent [24]. The recellularization process also needs to be optimized [23]. Decellularized scaffolds have been found to have traces of cellular components, such as nuclear DNA and cytoplasmic components, as well as ECM proteins that can trigger an immune response in patients [24]. Specifically, if this tissue is from animals the immune response needs to be analyzed and mitigated [23]. Recellularization of the tissue scaffold requires multiple cell types and proper cellular function. However, differentiation procedures produce impure cell populations and are overall inefficient [24]. Additionally, a large number of cells are needed to reseed the scaffolds, and expansion of cells is expensive and time-consuming [19], [24]. There are also limited points of access to reintroduce cells into the decellularized scaffold [24]. Finally, there is an inability to introduce cells to the deeper regions of decellularized scaffolds [25].

2.4 Microneedles

Microneedles utilize a transdermal technique to deliver drugs, vaccines, or other bioactive molecules to a patient, as well as collect signals and substances from the patient [26].

Microneedles consist of micron size needles, usually 50-900 micrometers with a diameter of fewer than 300 micrometers that are arranged in arrays [27]. Microneedles can be classified as hollow, solid, coated solid, dissolvable, or hydrogel, as shown in Figure 2.3. Hollow microneedles have an internal bore that allows drugs and other substances to be transported into the layers of the skin. A constant flow rate is essential for the delivery of drugs using these microneedles. Solid, uncoated microneedles form pores to create channels. These channels can increase the permeation of drugs and other solutions into the skin. Solid, coated microneedles are coated with a drug at different thicknesses. This type of microneedle allows for rapid, continuous release of the drug into the skin. Dissolvable microneedles are made of a soluble, biocompatible polymer that dissolves following contact with interstitial fluids to release drugs or other substances. Hydrogel microneedles utilize a crosslinked polymer that takes in interstitial fluid from surrounding tissue. As the microneedles become swollen, the drugs diffuse from the needle [27], [28].

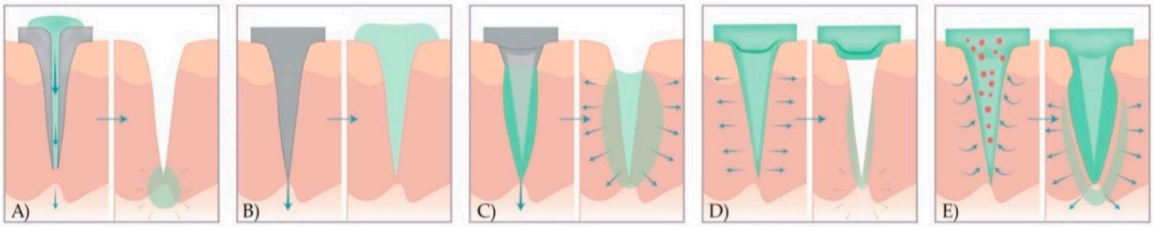

Figure 2.3: Classifications of Microneedles. Panel A shows hollow microneedles, Panel B shows solid microneedles, Panel C shows solid coated microneedles, Panel D shows dissolving microneedles, and Panel E shows hydrogel microneedles [27].

Microneedles can be made from a variety of different materials using different manufacturing methods. The material used to fabricate the microneedle will impact its properties [28]. Common materials used to produce microneedles include silicon, metals, such as stainless steel and titanium, ceramics, silica glass, carbohydrates, and polymers. Polymers commonly used to produce microneedles include polylactic acid (PLA), poly(lactic-co-glycolic acid) (PLGA), polyglycolic acid (PGA), poly(vinyl alcohol) (PVA), poly(carbonate), and poly(vinylpyrrolidone) (PVP) [27], [28]. These materials and the type of microneedle being produced impact the fabrication method used [28]. Microelectromechanical systems (MEMS) can produce microneedles in a three-step process of deposition, patterning, and etching materials. One such MEMS production method is photolithography, where an opaque mask is used to create a pattern. Another method to produce microneedles, usually those made of metal materials, is laser cutting. The shape of the microneedles is cut based on a CAD model using a laser beam. Laser ablation can also fabricate microneedles from metals using light pulses to form arrays. Additionally, micromolding can be utilized to produce microneedles. In this method, a liquid polymer solution is poured into a previously fabricated mold for the microneedles [27]. Air is removed from the molds and then they are dried in an oven. Atomized spraying utilizes a nozzle connected to a source of air to fill in molds with a liquid sugar or polymer solution.

Microneedles can also be fabricated using the droplet-born air blowing method (DAB), which shapes polymer drops into microneedles. The pulling pipettes method creates hollow glass microneedles by pulling glass pipettes that have been exposed to high temperatures. Additive manufacturing, or 3D printing, is being looked into for use in microneedle production as well. Additive manufacturing uses a 3D CAD model that is printed in layers through fusing or deposition of the material being used [27].

2.4.1 Advantages and Limitations of Microneedle Use

Microneedles decrease pain and damage to tissue that is often caused by conventional hypodermic needles by not reaching nerve endings [26], [27]. Additionally, microneedles offer the opportunity for a personalized drug delivery system [27]. Each type of microneedle is associated with its own benefits. Hollow microneedles are low-cost and accurately release drugs. Solid microneedles allow for the rapid delivery of drugs. Solid coated microneedles allow for a one-step application process. Dissolvable microneedles allow for control of drug delivery. In addition, this type of microneedle is less sharp and is easily degradable. Hydrogel microneedles leave the skin undamaged following removal. They also allow for adjustments during drug delivery by modifying the hydrogel density. Additionally, hydrogel microneedles reduce infection transmission [27].

While microneedles have many advantages over other transdermal technologies, they also have some reported limitations. Due to the needles being small and thin, there have been cases of the needle tips breaking off. This has the potential of staying inside the human skin and causing health complications. Further, there have been some issues of skin irritation or allergy due to a patient having sensitive skin [28]. In addition, a limitation of hollow microneedles is the resistance of flow that can occur within the tissue. A drawback of the solid, coated microneedles is that there are limitations to the amount of drug that the microneedles can be coated with. Dissolvable microneedles are limited due to the deposition of polymers that can occur. In addition, hydrogel microneedles can lead to potential side effects if they dissolve in the skin [27]. Finally, many current fabrication methods are high cost and labor-intensive [26].

2.5 Current Analytical Models

2.5.1 Mechanical Studies

Mechanical testing needs to be performed on microneedles to ensure that they can penetrate tissue without damage to the tissue or the needles. In previous studies, microneedles underwent insertion force tests as well as failure force tests. A variety of tests have been completed to measure the insertion force of the microneedles [28]. One commonly used test is dye marking, where dye was coated on the needles prior to insertion. Following insertion and removal of the needles, the site of insertion is inspected with a microscope. Force displacement tests and electrical measurements have also been used to determine the insertion force. Force-displacement tests apply a compressive force to the microneedles and the displacement of the microneedles, the length of time the test is performed, and the forces applied are recorded. Then,

a force-displacement curve can be created to determine the appropriate insertion force. Failure force is another relevant mechanical test performed on microneedles. The failure force can be determined by pressing the microneedles against a rigid surface and recording the force applied at failure. Failure is quantified when the needle breaks or buckles on the central axis. Additionally, failure can be quantified by bending or shearing. The ratio of the force the microneedle fails at and the force required to penetrate tissue gives a safety factor, and a larger factor is most desirable in microneedle designs [28], [29].

The mechanical properties of the decellularized tissue scaffold will impact the force applied to the microneedle system. A previous study used uniaxial testing to measure the mechanical properties of the decellularized tissue that the microneedles will be inserted into. In these uniaxial tests, tissue samples that had been previously decellularized and rehydrated were placed into two tensile clamps, and force and displacement were recorded. Properties of the tissue such as Young's modulus, maximum force, and maximum elongation were determined based on force and displacement. Additionally, the stress was calculated with the applied load from these uniaxial tests and divided by the pre-decellularized measurements. The strain was found by dividing the extension of the scaffold by the length of the pre-decellularized scaffold. Knowing the mechanical properties of the tissue can ensure that the microneedles have the necessary properties to successfully penetrate the tissue [30].

2.5.2 Cell Viability and Proliferation

Previous studies have utilized cell-based assays to measure cell viability and proliferation for determining if the microneedle design and the decellularized scaffold were not cytotoxic to cells [31]–[34]. Cell-based assays measure markers of viable cells, proliferating cells, and cytotoxic effects on cells [35]. Cell viability assays measure the number of living cells, while cell proliferation assays measure the response of cells to treatment. Commonly used cell-based assays fall into four main categories: tetrazolium reduction, resazurin reduction, protease activity, and ATP assays [35]. Two commonly used tetrazolium reduction assays are MTT and MTS assays. During an MTT assay, metabolically active cells convert MTT into a purple formazan product. A plate reader at 570 nm is used to measure absorbance values for this product. The signal detected by the plate reader depends on the concentration of MTT, incubation period, metabolic activity of cells, and the number of cells. Dead cells are differentiated by their inability to create the formazan product [35]. MTS is another tetrazolium assay, but it is more convenient because the formazan produced is soluble in cell culture media, eliminating the need for additional reagents. The absorbances values in an MTS assay are measured at 490 nm on a plate reader. The advantage of the tetrazolium assays is that the absorbance can be measured multiple times during incubation [35].

During resazurin reduction assays, metabolically active cells reduce resazurin to produce resorufin, a fluorescent pink product. Due to proportionality between the number of viable cells and resorufin product, fluorescence at 560 nm excitation and 590 nm emission is often measured for quantification of viable cells. Absorbance can be measured as well, but it is less sensitive than fluorescence measurements. Resazurin reduction assays are less expensive and more

sensitive than a tetrazolium assay [35]. A commonly used resazurin assay is an alamarBlue assay, which can measure viability and proliferation. An alamarBlue assay is beneficial because it is non-destructive, meaning viability can be measured over an extended time. Metabolically active cells reduce the alamarBlue leading to a change in color from blue to fluorescent red [36].

Protease activity can be used to measure the number of viable cells. A protease substrate, GF-AFC, that can penetrate the cell and generate a fluorescent signal following protease detection is utilized in these assays. The substrate used in the protease assays is non-toxic to cells, and long-term exposure will not alter viability measurements. Additionally, a signal can be measured faster with the protease activity assays than with tetrazolium assays [35].

ATP assays measure the presence of ATP with firefly luciferase. The loss of membrane integrity in cells occurs by the application of a detergent that lyses the cells. Then, ATPase inhibitors stabilize any ATP released from the cells to enable a reaction with the luciferase. This luminescent signal is measured and is proportional to the number of viable cells because ATP is a marker of viable cells. An advantage of using an ATP assay is that it is the quickest and most sensitive of the assay types [35]. A specific type of ATP assay is Cell Titer Glo Luminescent Cell Viability Assay. This type of assay reduces the number of steps involved with a homogenous mixture format that is directly added to the plate. The luminescent signal produced in the assay is directly proportional to the amount of ATP, which is representative of the number of metabolically active cells. The luminescent signal can be measured using a plate reader [37].

Other cell-based assays specifically used in previous microneedle studies include a LIVE/DEAD Viability/Cytotoxicity Assay, also known as a calcein AM/ethidium homodimer-1 viability assay, and a trypan blue exclusion assay [31]–[34]. LIVE/DEAD assays use two-color fluorescence to differentiate live and dead cells. A fluorescent green signal is produced when live cells convert non-fluorescent calcein AM to fluorescent calcein. Dead cells are detected when ethidium homodimer-1 enters damaged cells and produces a fluorescent red signal. A plate reader can be used to measure this fluorescent signal. This type of assay is advantageous because it is quick, inexpensive, and more sensitive to cytotoxicity [38]. Alternatively, a trypan blue exclusion assay utilizes light microscopy to quantify viable cells. Through this method, cells are suspended in PBS with trypan blue to determine the percentage of viable cells. Viable cells in trypan blue exclusion assays have a clear cytoplasm because the intact cell membrane excludes the blue dye, while dead cells have a blue cytoplasm. This methodology is advantageous because it is simple and rapid. However, this assay is limited because viability is indirectly measured based on membrane integrity [39].

2.5.3 Histological Analysis

Histology utilizes microscopy to study tissue characteristics and cell structures. During the histology process, fixation occurs when chemicals preserve the tissue and cell structure from degrading. Paraffin-formalin is often used during the fixation step [40]. Dehydration removes water from the tissue for solidification using ethanol, and xylene clears both the ethanol and paraffin wax. During the embedding phase, paraffin wax is used. A microtome is used to section

the tissue slices after it has been embedded. Histological stains aid in the analysis of tissue by highlighting features of the tissue. A common stain used in histology is hematoxylin and eosin (H&E). Hematoxylin stains the cells' nuclei blue, and eosin stains the extracellular matrix and cytoplasm of the cells pink [40]. Previous studies have used histology to observe tissue after treatment with microneedles and observe the insertion depth of the microneedles [28], [32], [33]. Other studies analyze decellularized tissue samples with histology to detect cell components [30].

2.5.4 Finite Element Analysis for Flow Rate

Previous microneedle studies have used flow rate analysis software to simulate volumetric flow rate and fluid velocity through microneedle designs [31], [41]. This software will be used to simulate the volumetric flow rate of liquid through our models. Not only are this software capable of determining flow rates, but they are also capable of measuring the loads associated with the insertion of the microneedles into the skin. A software with the capability to simulate fluid flow and loads associated with microneedle insertion is the ANSYS Finite Element Analysis Software. This software provides values such as the maximum length of the microneedles to reach desired depths and not break upon skin penetration. Additionally, the simulation can be used to determine the pressure contours around the inlet of the microneedle to reach the appropriate flow rate and velocity of the fluid through the needle [41]. This software is helpful in both saving time and eliminating waste by determining these values electronically as opposed to additional testing. Further, this simulation helps determine which designs are feasible prior to prototyping, which also limits unnecessary resource use and time. Another software that can be utilized for flow rate simulation is SolidWorks Flow Simulator, which uses Navier-Stokes equations and a finite volume method to solve for flow rate [31].

2.5.5 Structural Evaluation

To analyze microneedle needle geometry and dimensions such as tip radius, length, and height, a variety of microscopy methods can be used. Both optical and electrical microscopy are commonly utilized [28]. Confocal laser microscopy can also be used for dimensional analysis by producing high-resolution images [28], [42]. However, a wider variety of previous microneedle studies have used scanning electron microscopy (SEM) to analyze needle geometry [28], [31], [42]–[45]. Scanning electron microscopy (SEM) uses an electron beam to interact with atoms in the microneedles to collect information related to surface topography, crystalline structure, composition, and electrical behavior [28], [46]. SEM has also been used to analyze the 3D structure of both native tissue (controls) and decellularized tissue. Images produced by SEM can show a lack of cells in decellularized tissue and the presence of microfibers in the tissue [47].

2.6 Microneedle Prior Art and Gold Standards

Microneedles are used for a variety of applications including cosmetics, disease diagnosis, drug delivery, and disease treatment [48]. Many cosmetic microneedles aim to reduce

signs of aging, scarring, stretch marks, pores, and other skin imperfections by signaling your skin to produce collagen and elastin. Cosmetic microneedles are limited in needle depth. The Dr. Pen M8 Microneedling Pen can only reach a depth of up to 2.5mm, and the Ora Face Microneedle Dermal Roller System reaches a depth of 0.5mm [49], [50]. Additionally, these two cosmetic needles are solid needles that do not deliver cells to a specific site. These products are also expensive, with the Dr. Pen M8 Microneedling Pen selling for almost $200 [49]. Microneedle patches have also been developed to transport cosmetics, such as retinyl retinoate and ascorbic acid, into the skin to reduce the risk of allergy [48]. There is also a patented microneedle-based cell delivery system used for cosmetic benefits. In this device, a microneedle extracts and transfers skin cells to other parts of the skin. The skin cells include melanocytes, fibroblasts, and keratinocytes. A benefit of this microneedle is that it reduces pain and scarring. A drawback of this microneedle design is that the maximum penetration depth is 1 mm, which limits its applicability [51].

Microneedle electrodes and patches have recently been developed to diagnose a variety of diseases [48]. There have also been developments of microneedle patches for drug delivery and disease treatment [48]. For example, the Zosano Intracutaneous Microneedle System utilizes a reusable applicator and a microneedle patch to deliver drugs through the skin. The needles in the system penetrate to a shallow depth to avoid pain in the patient. This technology also allows for faster drug absorption than oral administration [52]. However, this technology cannot penetrate to a sufficient depth to recellularize thick tissue. Corium's MicroCor technology utilizes dissolvable microneedles for biologic delivery through the skin. This technology can be self-administered and only needs to be worn for a short time [53]. Similar to the Zosano microneedles, the MicroCor technology cannot penetrate through tissue thicker than the epidermal layer of the skin. Microneedle patches that regulate blood glucose levels and deliver insulin in type 1 diabetics have also been developed. For example, the BD Micro-Fine Ultra 4mm Pen needle is a 32 gauge needle used to inject insulin that reduces the pain related to injections, reduces the risk of hypoglycemia, and improves the absorption of insulin [54]. This microneedle is applied solely to penetration through the skin; therefore, it cannot penetrate thicker, deeper tissue. The use of microneedles to deliver vaccines is also being studied, such as the delivery of inactivated influenza viruses using biocompatible microneedles [48]. NanoPass Technologies' MicronJet hollow microneedles deliver drugs and vaccines through the skin. This product reduces pain and shows improved immunological results compared to subcutaneous or intramuscular drug delivery [55] However, the microneedle is less than 1mm, which impedes its ability to reach deeper tissue. While there are many applications and microneedle products on the market, a majority of them are cosmetic-focused and do not penetrate an adequate depth for the recellularization of tissue. Additionally, these microneedles have not been previously used for cell delivery to deep tissue.

CHAPTER 3: PROJECT STRATEGY

3.1 Initial Client Statement

The use of decellularized scaffolds is a promising approach to repairing large volume muscle injuries and burn injuries. There are two options for using decellularized tissue scaffolds. The first option is to transplant a decellularized patch to the injured area to allow native cells to migrate and repopulate the patch. The alternative option is to repopulate the patch with cells in vitro prior to transplantation. One of the biggest challenges to the latter approach is the inability to efficiently repopulate cells to deeper regions of the decellularized tissue patches. Therefore, there is a need to be able to repopulate thick decellularized tissue with cells. The initial client statement provided by the project advisor was to develop a micro/nano needle cell injection device to deliver precise volumes of cell suspension to various tissue thicknesses from 1 to 5 centimeters [25].

3.2 Design Requirements (Technical)

3.2.1 Design Objectives, Constraints, and User Requirements

Based on the initial client statement, the device must deliver cells to decellularized tissue patches one centimeter deep. The device must have a storage component to house cells prior to their release. The design should preserve cell viability and disperse the cells evenly throughout decellularized tissue scaffolds. Additionally, the flow rate of the cell suspension fluid must be controlled as it enters the decellularized tissue to allow for cell adhesion. The penetration mechanism of the device should be removable from the scaffold. The device needs to be effective for many applications, such as various decellularized tissue scaffolds for different wound types. One design constraint is the need for cell viability [56]. Another constraint is that the device must reach a depth of at least one centimeter. In terms of user requirements, the device should be easy to use. Researchers or healthcare providers at various experience levels should easily understand how to utilize the device for cell delivery to decellularized tissue.

3.2.2 Functions and Sub-Functions

Based on the need statement, we developed three functions of our device with their respective sub-functions, shown in Table 3.1. The first function is that the device must be able to deliver cells. Based on this function, we developed the sub-function that the device must preserve cell viability to ensure the delivery of live cells. The device also needed to control the flow rate to allow the cells enough time to adhere to the decellularized tissue scaffold. Additionally, we determined that the device needs to evenly spread the cells throughout the tissue scaffold as they are delivered. Finally, the device needs to hold the cells prior to their release to allow for the principal function of cell delivery.

The second crucial function of the device is that it must allow cells to reach a depth of one to two centimeters. Multiple sub-functions are necessary to produce this overall function. First, the design must access various depths to allow for cell delivery to different tissue thicknesses. Additionally, to deliver cells to the appropriate depth, the penetration system must

be removed from the decellularized tissue scaffold without causing damage to the tissue. Finally, the penetration system needs to have a high degree of structural integrity to ensure that it does not break upon entering the scaffold.

This second function directly coincides with the third function because the device must function in a way that penetrates tissue. To penetrate the tissue, the device must withstand the initial penetration force of the tissue without breaking. The penetration system also needs to maintain its structural integrity with the increasing pressure associated with the penetration and release of cells. Lastly, the penetration system must not damage the scaffold upon insertion but still allow for cell delivery. Specifically, for microneedle penetration, the needles must be small enough to not damage the decellularized tissue scaffold, but large enough to allow cells to flow through. Table 3.1 summarizes the principal functions and the respective sub-functions of the device.

Table 3.1 Design Functions and Sub-functions. There are three principal functions with respective sub-functions that contribute to the overall design. The position of each sub-function is below the overarching function to which it contributes.

Deliver Cells	Reach Depths of One Centimeter	Penetrate Tissue
Preserve cell viability	Reach variety of depths	Penetration system does not break upon entering the decellularized scaffold
Controls rate of flow for cell adhesion and integrity	Ability to remove penetration system from the decellularized scaffold	Maintain structural integrity of the design under increasing pressure
Disperse cells evenly throughout the scaffold	Penetration system can reach one centimeter without breakage	Limit damage of the scaffold upon penetration
Temporarily hold and store cells prior to release		

3.2.3 Systems and Subsystems

Based on the need statement, we identified several systems and subsystems necessary for the device. Each overall system and subsystems transform inputs into outputs to meet the functional requirements of the device. The entire device is a system that needs to deliver cells to decellularized tissue scaffolds. Within this system, there is a penetration subsystem, cell storage subsystem, pressure or delivery subsystem, and a controlled removal subsystem. The system flow chart, Figure 3.1, details the inputs and outputs of each subsystem to ultimately input cells and output repopulated tissue patches.

The system must have a cell storage subsystem to house cells prior to delivery. The target cells and cell media that these cells grow in are both inputs for this cell storage subsystem. The cell storage subsystem would satisfy the necessary sub-function of temporarily holding the cells prior to delivery. In conjunction, the system needs a penetration subsystem to enter the scaffold

and access deeper parts of the decellularized tissue scaffold. This subsystem would take pressure, or some trigger energy, to enter the tissue scaffold and reach desired depths without damaging the device, scaffold, or cells themselves. The penetration subsystem would satisfy the functional requirements of reaching various depths, maintaining device integrity upon entry, and maintaining scaffold integrity upon entry. Both tissue penetration and cell storage processes will lead to the release of cells. Once the device is positioned at the desired depths, the device then needs a pressure or delivery subsystem to initiate the removal of cells from the device into the decellularized scaffold. The output of this subsystem is the release of cells. The pressure or delivery subsystem would satisfy the functional requirement of controlling the rate of cell release to maximize cell adhesion and cell viability. The final subsystem is a controlled removal subsystem. This subsystem could satisfy the functional requirements of dispersing cells, reaching various depths, and removing the device from the scaffold. Once the device is removed, the repopulated tissue scaffold is the output product.

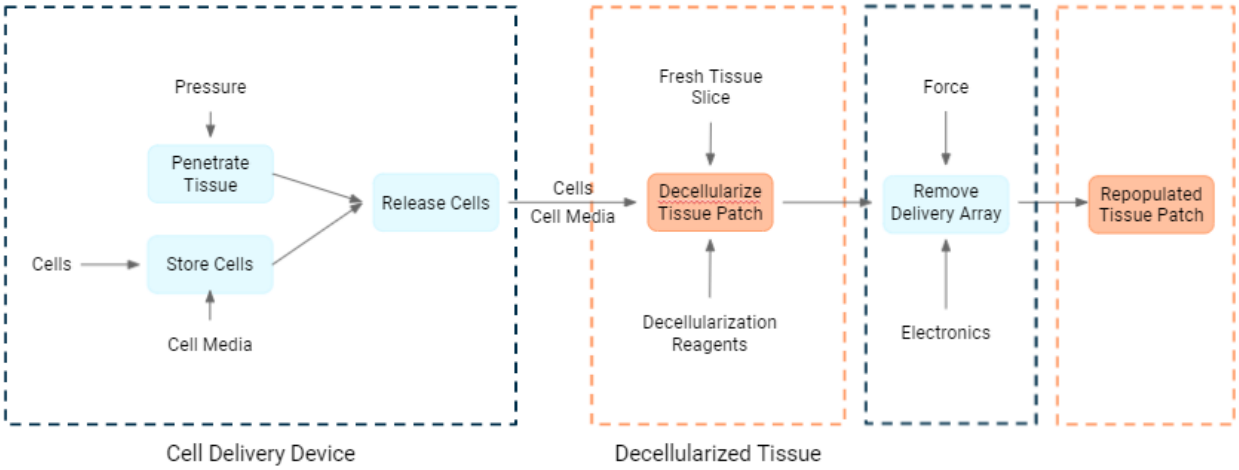

Figure 3.1: System Flow Chart. This flow chart details the functions met by each subsystem and how each subsystem contributes to the overall system. This device must take cells, cell media, and pressure and repopulate decellularized tissue patches with depths of one to five centimeters. The repopulated patches must have at least 80% cell viability [56]. The blue dashed boxes indicate subsystem interactions within the device itself, and the orange dashed boxes indicate subsystem interactions with the decellularized tissue scaffold.

3.2.4 Functional and Performance Specifications

Our team determined a number of functional and performance specifications to be considered for our final device. These specifications are outlined in Table 3.2.

Table 3.2: Functional and Performance Specifications.

Functional Specification	Performance Specification
Target deep into decellularized tissue with cells.	Penetrate 1 centimeter deep into decellularized tissue [25].
Maintain cell viability.	Achieve cell viability of 80-90% [56].
Adequate microneedle width.	Maximum microneedle width of 350 microns.
Temporarily hold cells for storage.	Adequate temperature of 25-37°C to support cell survival for a short period of time. Accommodate necessary volume of cells and media needed to achieve cell viability.

3.3 Design Requirements (Standards)

Our team will need to consider several standards related to medical devices and tissue scaffolds. One such standard is the international standard from ISO 10933-1: "Biological evaluation of medical devices- Part 1: Evaluation and testing with a risk management process." This standard requires that medical devices evaluated for biocompatibility must also have associated risk management processes. During this process, the material used in the device, the manufacturing process, the intended clinical use of the device, and the length of exposure to the device are evaluated. This evaluation helps to expose possible biocompatibility risks such as chemical toxicity and physical properties of the device that elicit unwanted biological responses. This risk management process should be performed on the final product of the device. For the device to be considered biocompatible, the materials used should not lead to adverse effects locally and systemically, be a carcinogen, or lead to development issues [57].

The ASTM F3206-17 Standard Guide for Assessing Medical Device Cytocompatibility with Delivered Cellular Therapies. This standard describes parameters that need to be considered for *in vitro* testing on a device that delivers cellular products to determine if the cells have been impacted through delivery. The standard encourages testing human cell lines that are related to the purpose of the device. Additionally, the cell morphology, density, and dissociation method needed for adherent cells should be characterized prior to testing. Positive and negative controls should be used in cytocompatibility testing as well. To assess the effect on flow rate out of the device on the cells, the standard suggests assessing the maximum and minimum flow rates for the device. The standard requires that the devices be tested in the final form. According to this standard, testing the cytocompatibility of the device should measure total cell recovery, cell viability, and cell function following delivery [58].

Numerous standards exist related to tissue scaffolds. One standard our team will consider in our final design is ASTM F2150 Standard Guide for Characterization and Testing of Biomaterial Scaffolds Used in Tissue-Engineered Medical Products. This guide outlines test methods to characterize the physical, chemical, mechanical and surface properties of tissue scaffolds. Additionally, this standard addresses characterization of sterilization techniques, tests

related to degradability and absorbability of the scaffolds, and biological testing. The chemical tests outlined in the guide include identifying impurities in the scaffold, determining solvents for dissolving the scaffold, and determining the molar mass of the scaffold. Physical tests outlined in the guide determine information about the scaffold such as porosity, density, crystallinity, or surface properties. The mechanical testing options outlined in this standard can help determine compressive, tensile, bending, and creep properties of the scaffold [59].

Another standard related to tissue scaffolds that our team will consider is ASTM F2739 Standard Guide for Quantitating Cell Viability Within Biomaterial Scaffolds. This standard provides testing methods for assessing viable and non-viable cells in a variety of biomaterial scaffolds *in vitro* or after the scaffolds have been retrieved following implantation. Some of the test methods also differentiate between cells that are proliferating and those that are not. The tests used to quantify cell viability outlined by this standard are split into four main measurement types: total cell number, live cell number, live/dead ratios, and imaging the density and morphology of the cells. DNA and crystal violet assays can be used to measure total cell number. Metabolic assays, MTT assays, MTS assays, Alamar Blue assays, Neutral Red, glucose consumption, dye exclusion, and trypan blue can all be used to count the number of live cells. Dual fluorescent stains and dye exclusion assays are used to determine live/dead ratios. Finally, histology, confocal microscopy, and scanning electron microscopy have been outlined in this standard for cell imaging techniques [60].

ASTM F2603 is a guide for interpreting images of polymeric tissue scaffolds. Depending on our validation and verification methods, understanding imaging of the repopulated tissue scaffolds will be a necessary step. This standard provides guidelines for how to use imaging of scaffolds to obtain quantitative data. The scaffolds used in this guide are polymeric; therefore, the guidelines cannot be directly applied to the natural, decellularized scaffolds for our testing. The standard provides insight into particle detection and analysis, which is still applicable to our application. It also outlines necessary environmental and microscope setting factors for optimal image capturing and analysis. Finally, this standard outlines measurement practices to obtain objective, quantifiable data based on the images of samples [61].

The Darcy permeability coefficient of our tissue scaffolds is vital in determining the necessary viscosity of the cell suspension used. ASTM F2952-14 describes the standard testing methods used to identify this coefficient of any porous tissue scaffold. The pressure gradient that could cause the cells and suspension to flow through the scaffold is the result of the weight of the cells and cell suspension. This method is non-destructive and non-contaminating, meaning that this can be done on a scaffold just before it is repopulated with cells. A limitation of this method is that steady-state flow needs to be achieved; therefore, if any damage or voids are present in the scaffolding, then the result will not be accurate. There also must be a linear relationship between the volume flowing through the scaffold and the differential pressure drop across the scaffold. These tests can be completed using deionized water [62].

The ISO 80369-7:2021 standard was used to design the connections within the device assembly [63].

3.4 Revised Client Statement

Following background research and discussions with the client, our team determined that our client needs a system to populate one centimeter thick decellularized tissue patches with suspended target cells.

3.5 Management Approach

A number of tasks were outlined, as well as the start date and end date we planned to complete each item. A majority of tasks were assigned to the entire team. Many tasks were interrelated and relied on each other. For example, evaluating the effectiveness of decellularization procedures could not occur until the decellularization procedures have all been performed. The Gantt chart, Appendix G, outlines each specific task and the respective timeframe for completion.

CHAPTER 4: DESIGN PROCESS

4.1 Needs Analysis

Our team used a pairwise comparison chart (PCC), Table 4.1, to compare the product specifications to one another. The total score column indicates the specifications that are most important to incorporate in our final device. Specifically, even delivery of cells to the decellularized tissue and the ability of our final device to penetrate the tissue are the two most important design specifications. Ensuring that the structural integrity of the device and the scaffold remains intact after penetration is another vital requirement according to the PCC. The least important requirements for our device are related to reusability and cost. The PCC allowed our team to compare and determine the weights of the design requirements for our design selection matrix, Table 4.2. A higher total score in the PCC led to a higher weighted design requirement.

Table 4.1: Pairwise Comparison Chart of Design Requirements. Scores are ranked on a scale of 0-1, with 0 being less important, ½ being equally important and 1 being more important.

OBJECTIVE	Deliver cells evenly	Reusable	Able to Penetrate	Broad Application	Inexpensive	Easy to use	Structural Integrity	Biocompatible	Maximize cell viability	TOTAL SCORE
Deliver cells evenly	X	1	½	1	1	1	½	1	1	7
Reusable	0	X	0	0	1	0	0	0	0	1
Able to penetrate	½	1	X	1	1	1	½	1	1	7
Broad Application	0	1	0	X	1	1	0	0	0	3
Inexpensive	0	0	0	0	X	0	0	0	0	0
Easy to use	0	1	0	1	1	X	0	0	0	3
Structural Integrity of device and scaffold	½	1	½	0	1	1	X	1	1	6
Biocompatible	0	1	0	1	1	1	0	X	1	5
Maximize cell viability	0	1	0	1	1	1	0	0	X	4

Table 4.2: Weighted Design Requirements. This table allows our team to differentiate which design requirements are wanted and which ones are needed. A weight of five indicates a necessary design requirement and is the most important. In comparison, a weight of one represents a want and is the least important design requirement.

Requirement	Weight
Deliver Cells Evenly	5
Able to Penetrate	5
Structural Integrity of Device and Scaffold	4
Biocompatible	3
Maximize cell viability	2
Broad Application	2
Easy to Use	2
Reusable	1
Inexpensive	1

4.2 Concept Maps and Prototyping

To determine potential design solutions to address the need presented by the client, we utilized a concept map, Figure 4.1, to organize potential solutions into categories. Our possible design solutions fell into three main categories: mechanical penetration methods, diffusion-based penetration methods, and electrical-based penetration methods. Explanations of each design solution are in the following section, 4.3.

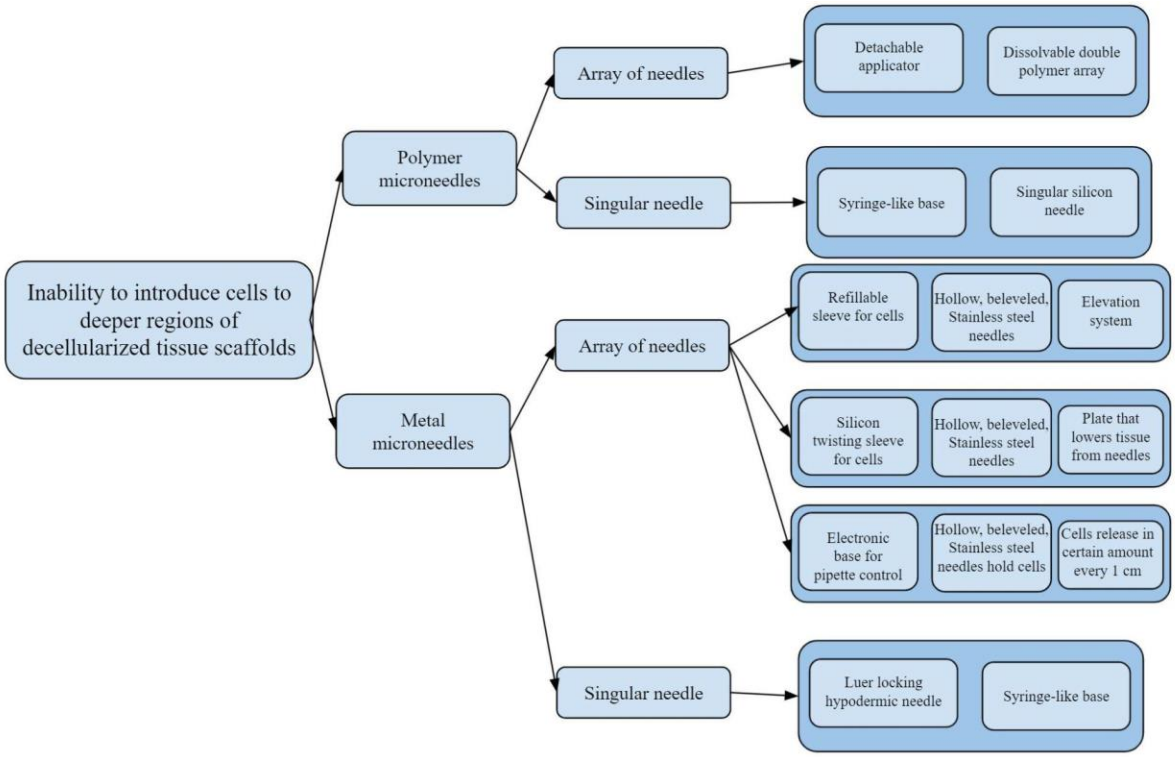

Figure 4.1: Concept Map. This map organizes potential design solutions.

4.3 Design Concepts

Based on our need statement, we brainstormed potential designs to deliver cells to thick decellularized tissue scaffolds. Our first design solution is microneedles that are made of a PLGA shell containing cells, media, and gelatin, shown in Figure 4.2. Previous microneedle studies utilized methacrylated gelatin, however UV exposure is needed to induce crosslinking and the UV light could have cytotoxic effects on the cells [33]. This led us to create a design that utilized gelatin material inside of the PLGA shells instead. Additionally, our PLGA shells would be larger than those in previous studies, with a length of at least one centimeter. These double polymer microneedles would be attached to a detachable applicator. The needles in this design would be organized in a 2 by 4 array for 8 total microneedles. These microneedles would dissolve in the decellularized tissue to release the cells.

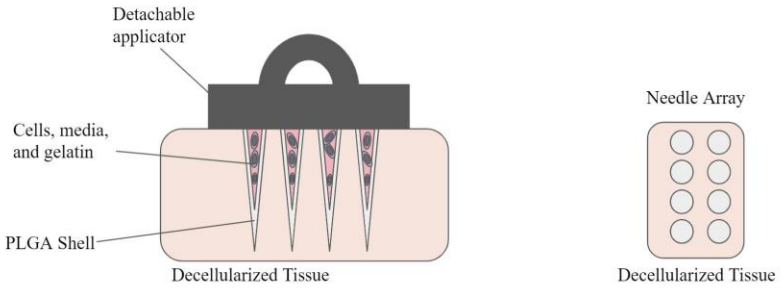

Figure 4.2: Double Polymer Dissolvable Microneedles

The second alternative design concept is a stainless steel microneedle array coupled with an elevation system, shown in Figure 4.3. The design would have a refillable sleeve that clicks into a syringe-like base and can be autoclaved for reuse. This refillable sleeve would be filled with cell and media suspension. The syringe-like base would be warmed via an electrical system to 37℃. A plunger would be inserted into the device once the sleeve had been added into the base to release the cells. The microneedles would be connected to a circular platform with a Luer lock to allow for a secure connection between the syringe-like base and the needles. It would also allow for detachment of the base from the needles. To evenly distribute the cells and allow for controlled removal of the microneedles, an elevation system connected to the base of the device would push the device out of the decellularized tissue as the cells are being delivered using a timed electrical system. The microneedles in this device would be hollow, beveled, and made of stainless steel. The needles would be arranged in a circular pattern of one, four, seven, and ten microneedles to create a total of 22 microneedles. The needles will be at least one centimeter in length. The radius of the hole of the microneedles will be no larger than 250 microns, but no less than 100 microns [64].

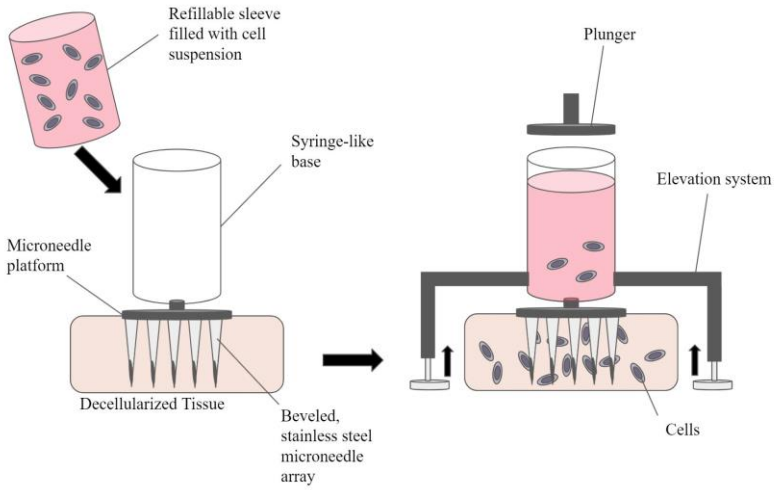

Figure 4.3: Stainless Steel Microneedle Array with Elevation System

The third alternative design concept is an assembly of five components: a silicone twisting container, an outer casing, compressed air influx, a plunger, and a detachable needle array, shown in Figure 4.4a. The cells and cell media are stored in a silicone, collapsible container. This container can be autoclaved for sanitation and collapses in a twisting motion as the plunger compresses it with increasing air pressure. There is a lip on the bottom of the container that prevents cells from contaminating the casing during use. The plunger is positioned just under the inlet for the compressed air with an interior lip and be flush with the casing. There is a detachable microneedle array attachment that can be changed out and discarded after use. The outer casing is made of a hard plastic and has a valve for a syringe or air compressor to attach via a Luer lock. The casing is also threaded on the bottom for the attachment and removal of the microneedle array. This delivery device will be paired with a movable platform to house the decellularized tissue during use, shown in Figure 4.4b. The tissue scaffold is held in place by a clamp that slides horizontally into place, ensuring no compressive forces are applied. The platform moves down at a steady rate as the delivery system is dispensing cells to allow for controlled spreading of cells throughout the scaffold.

a)

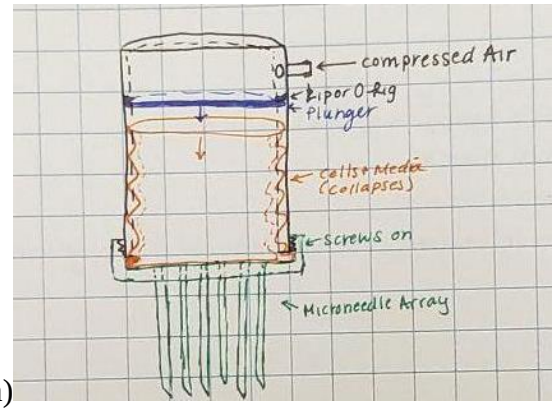

b)

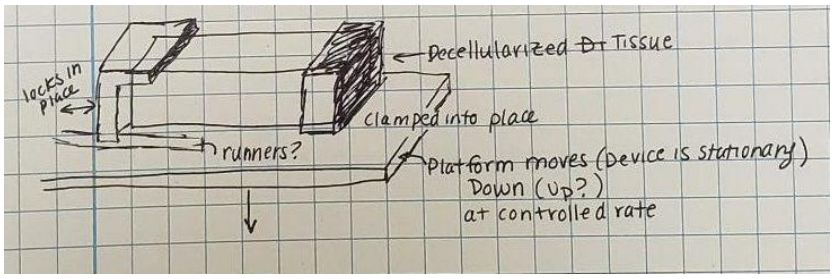

Figure 4.4: a) Twister with Air Compressor Delivery System. b) Twister with Air Compressor Platform.

Our final proposed alternative solution is an electronic pipette microneedle system, shown in Figure 4.5. An array of Luer locking, hollow, beveled microneedles fabricated from stainless steel would be attached to an electronic pipette. The electronic pipette system takes up the total amount of cell and media suspension needed to recellularize the tissue. Then, the pipetting system dispenses the cell and media suspension in an equal volume every time the

button is pressed. For example, the electronic system could disperse 1 mL of cells and media every centimeter throughout the decellularized scaffold. This would allow the microneedles to be moved up 0.5 to 1 centimeter between every button click, to allow for even dispersion of cells.

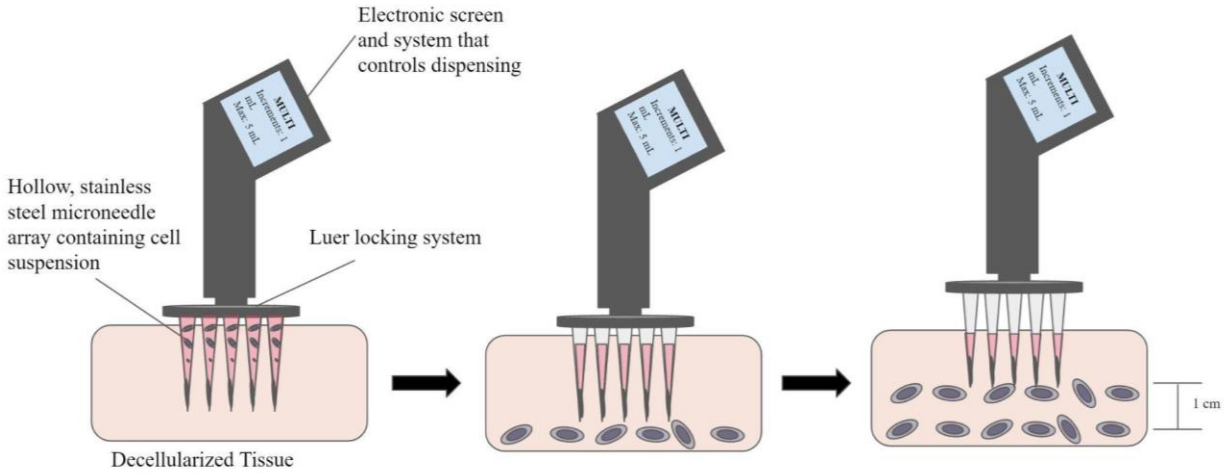

Figure 4.5: Electronic Pipette Microneedle System

4.4 Design Selection

We compared our three alternative design solutions to a baseline design to determine the optimal design solution. The baseline design that we chose was Zosano's Intracutaneous Patch Microneedle System. The Zosano device includes a reusable applicator and a microneedle patch for drug delivery through the skin. There are two thousand titanium microneedles on the patch, as well as an adhesive backing. The needles are approximately 500 micrometers long and are three times as wide as human hair. The needles are coated with the drug and deliver the drug by penetrating the outer layer of the epidermis, decreasing pain [52]. A design selection matrix, Table 4.3, was used to compare our design solutions to the baseline. Each alternative design was compared to the baseline using the weighted design requirements from the PCC. The baseline device received a score of 0 for all design requirements. Our alternative design solutions were scored on a scale of -1 to +1, with -1 being weaker than the baseline, 0 being equal to the baseline, and +1 being more effective than the baseline. The scores were weighted and totaled to determine a rank score for each design. The design consisting of a solid, bioresorbable needle array ranked the highest with a score of six.

Table 4.3: Design Selection Matrix. Designs were ranked -1, 0, or +1 for each requirement. The highest scoring design was chosen for prototyping.

Requirement	Weight	Baseline: Zosano Intracutaneous Patch Microneedle system	Design 1: Double Polymer Dissolvable Microneedles	Design 2: Elevation System	Design 3: Silicon Twister with Air Compressor	Design 4: Electronic Pipette Microneedle System
Deliver Cells Evenly	5	0	+1	+1	+1	+1
Able to Penetrate	5	0	-1	0	0	0
Structural Integrity of Device and Scaffold	4	0	-1	0	0	0
Biocompatible	3	0	0	0	0	0
Maximize cell viability	2	0	+1	+1	+1	+1
Broad Application	2	0	+1	+1	+1	+1
Easy to Use	2	0	-1	-1	0	-1
Reusable	1	0	0	0	0	0
Inexpensive	1	0	0	0	+1	0
TOTAL SCORE:		**0**	**-2**	**7**	**10**	**7**

Our team then created a model assembly of the selected design using SolidWorks, Figure 4.6. The device has five components: a silicone twisting container, an outer case, compressed air influx (syringe), a plunger, and a detachable needle array. The cap is detachable and customizable for compatible use with commercial microneedles or a custom microneedle array.

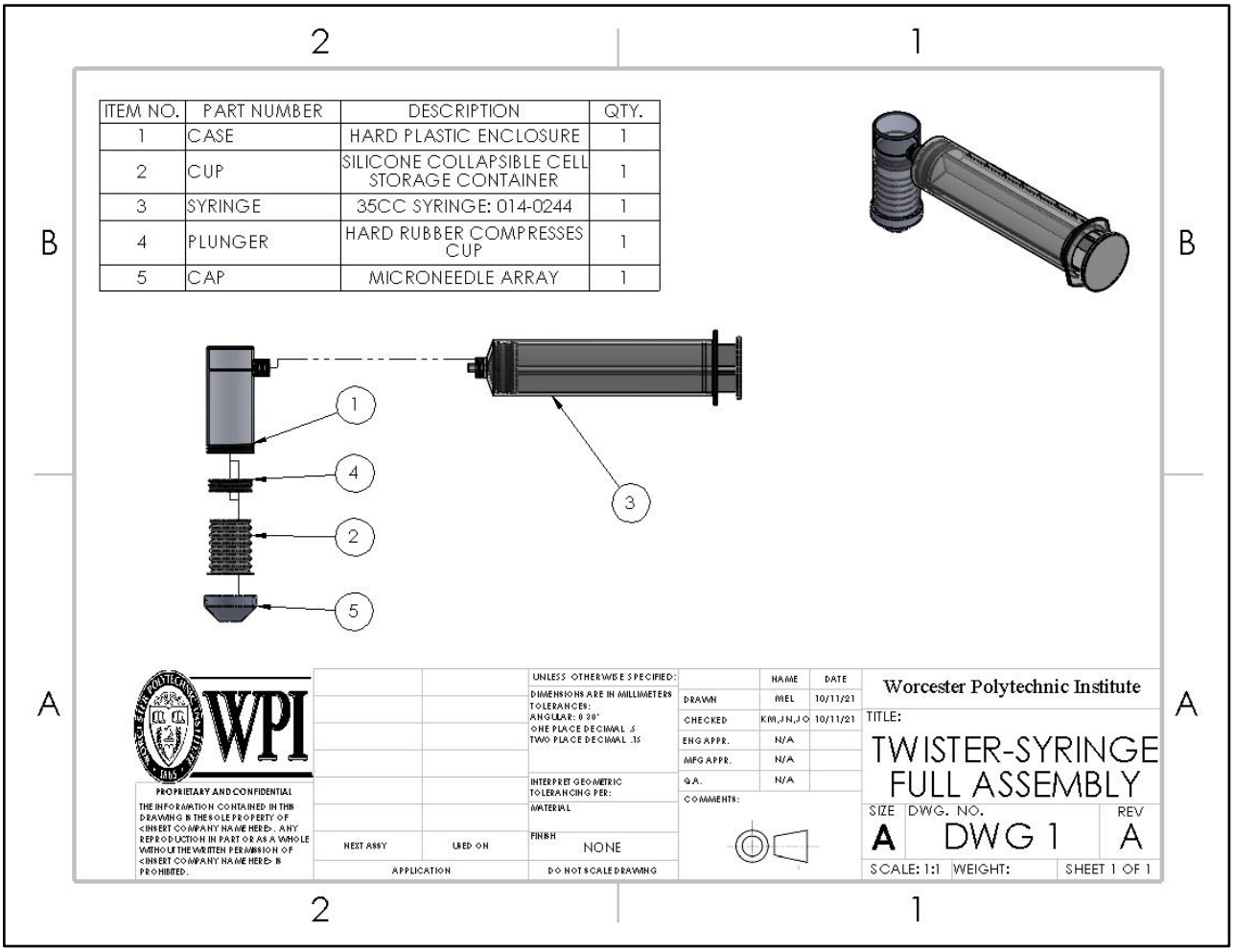

Figure 4.6. Silicon Twister with Syringe Assembly Drawing. The design was modeled in SolidWorks. The components can be easily exchanged during the prototyping process. This stationary delivery system is paired with the moving platform that lowers to allow for controlled spreading of cells throughout the tissue scaffold.

4.4.1 Means Table

Following the selection of our final design, our team utilized a means table, Table 4.4, to determine how to incorporate the design requirements, functional specifications, and performance specifications into the design. For each functional and performance specification, we identified three to four possible means as potential solutions. Our final device has individual or multiple means corresponding to each specification to achieve the overall functionality needed.

Table 4.4: Means Table. Outlines the specifications and the potential means to accomplish the specifications.

Functional Specification	Performance Specification	Means			
Deliver cells to varying depths of decellularized tissue.	Penetrate 1-2 centimeters deep into decellularized tissue [25].	Microneedle	Hypodermic needle	Absorbance with biocompatible material	
Maintain cell viability.	Achieve cell viability of 80-90% [56].	Storage container heats to 37°C	Autoclaved storage container	Appropriate growth medium	Appropriate pH
Adequate microneedle width.	Maximum microneedle width of 350 microns.	SLA 3D printed Mold	Metal Etching	Outsourcing fabrication	Premade needles
Temporarily holds cells for storage.	Adequate temperature of 25-37°C to support cell survival for a short period of time. Accommodate necessary volume of cells and media needed to achieve cell viability.	Syringe	Biocompatible polymer	Single-Use Pod	

4.5 Minimum Viable Product

Our team plans to use a minimum viable product (MVP) based on our leading design concept to begin the testing phase of our device. The complexity of the MVP device increases with each performed test until it satisfies all functional and performance specifications. Based on our need statement, our minimum viable product is a device that delivers cells. Cell delivery is the core function of our device; without cell delivery, we do not have a product.

4.6 Iterative Prototyping

The Silicone Twister with Syringe alternative design, described in Section 4.3, was pursued initially. The casing (#1 in Figure 4.6 in Section 4.4) was 3D printed out of PLA before simplifying the design. The simplified design utilizes a syringe pump, Figure 4.7, to control the dispensing rate of cell suspension into the tissue scaffold. A syringe is loaded with cell suspension and positioned in the syringe pump as shown. A blunt end, Luer locking adaptor (pink) is then attached to the syringe and tubing allows for isolated movement of the needle array, which is attached on the other end by another adaptor. The needle array has a complementary Luer locking feature to create a secure seal, Figure 4.8.

The option of creating a cell reservoir with 3D printed needles as one solid piece was explored, Figure 4.10. The LEAP program at WPI has a nanoscribe nano 3D printer. The nanoscribe has a resolution of 200 nm and the capacity to print up to 1 in. The resolution of the nanoscribe is smaller than our entire reservoir piece; therefore, we would need to just print a select number of holes, since resin 3D printers, such as the Formlabs Form 2 printer, do not have

the capacity to print to that resolution without the holes collapsing. The nanoscribe is also expensive for training and use: $35/hr for self-use, $85/hr for assisted and training use, and $10/hr for clean room use. Outsourcing costs were also outside of the budget, especially for an initial prototype. Additionally, the needles would need to be redesigned since the aspect ratio is very low and they would act as cantilever beams. Therefore, the needles need to be metal to maximize their structural integrity, and metallic 3D printing would have to be outsourced. For the initial working prototype, the team pursued commercial-off-the-shelf needles instead of custom needles.

A test piece for the fabrication of the microneedle array component, Figure 4.9, was printed in two different materials using a Formlabs Form 2 3D printer. The two materials investigated were the Dental and Durable resins. The Dental resin is biocompatible; however, it can undergo brittle failure depending on the application [65]. The Durable resin has more elasticity and can sustain repeated loading; however, it is not biocompatible [66]. The intention was to print the part in both materials and use CNC machining to drill precision through holes at a diameter equal to the outer diameter of the needles. Two different sized drill bits were tested, 0.3mm and 0.275mm, to determine the best fit for press-fitting 30 gauge needles into the holes. Once the 30 gauge, commercial-off-the-shelf needles were press-fitted into the varying holes, the fits were evaluated to determine which drill bit and corresponding tolerancing was needed for successful assembly. These fabrication trials also helped determine if the Dental material was too brittle, the feasibility of the intended fabrication process, and the necessary tools needed for this fabrication.

Figure 4.7. The New Era Pump System Inc. Syringe Pump from SyringePump.com (Model No. NE-300, Volts/Hz: 12V DC, Amperage: 0.75, Series No. 288793) is used to compress a 12mL syringe plunger at a steady rate. The syringe is connected to a 20g x ½" Luer stub adaptor, then a PVC tube, and another Luer stub adaptor. The second adaptor is attached to the needle reservoir, Figure 4.8. The inner diameter of the syringe and crosshead speed are set manually; therefore, these two values can be iterative.

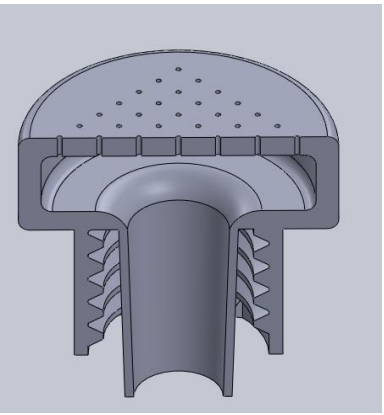

Figure 4.8. Section view of the microneedle array. The bottom threaded feature is the complimentary Luer lock design for the pink adaptor in Figure 4.7. Commercial, off the shelf microneedles will be press fit into the holes. This iteration utilizes 49, 30 gauge needles.

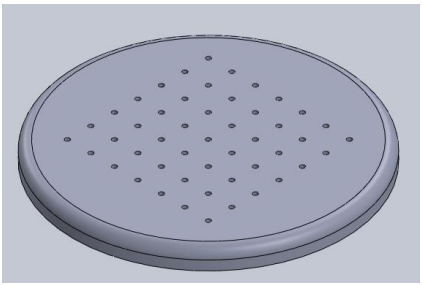

Figure 4.9. Testing piece for microneedle array assembly. This part was 3D printed using a Formlabs Form 2 printer. Two material resins were tested: Durable and Dental.

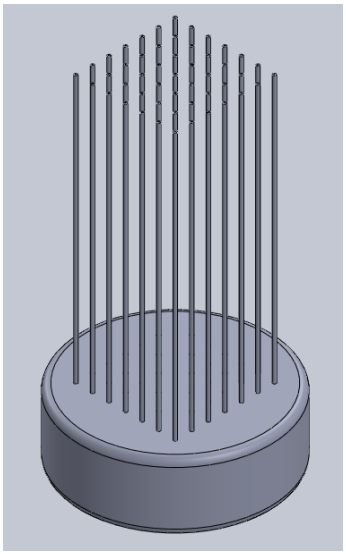

Figure 4.10. Custom, 2cm long needle array attached to cell suspension reservoir. The design would be fabricated as one entire piece.

CHAPTER 5: FINAL DESIGN AND DESIGN CONSIDERATIONS

5.1 Final Design

Based on the client statement, a microneedle reservoir that fit the design requirements was modeled using SolidWorks, Figure 5.1. Dimensional analysis determined the feasibility and functionality of each iteration of the device. It was determined that a reservoir system connected to a motor-driven syringe pump would allow for controlled dispensing of precise volumes of cell suspension into decellularized tissues. Drawings of each component made using SolidWorks per the ANSI standard are in Appendix F.

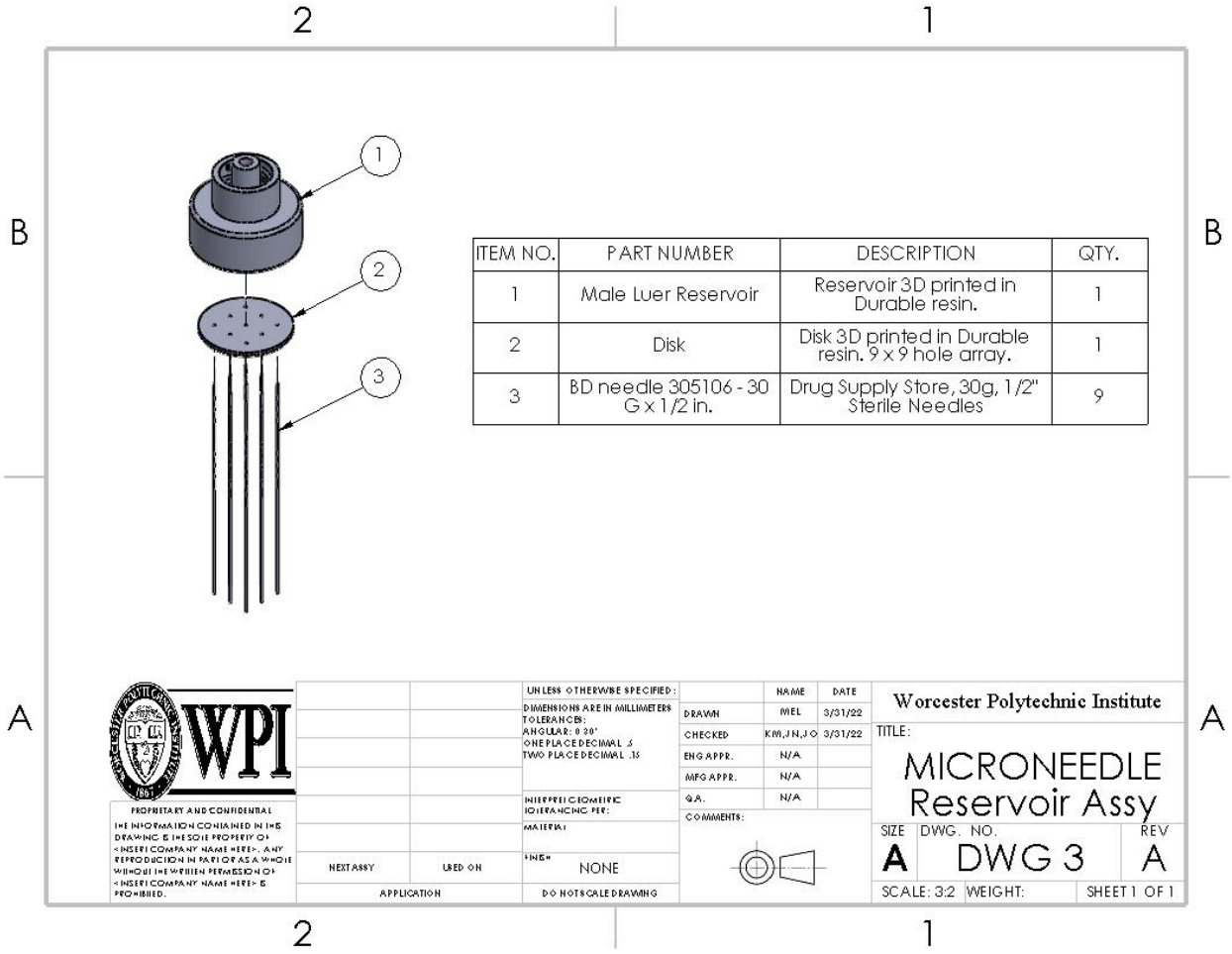

Figure 5.1: CAD drawing of exploded view of the reservoir assembly.

A two-part reservoir assembly was developed. Commercial, ½ inch long 30g needles were press-fit into the device. The reservoir was fabricated in two parts, a disk and a male Luer locking component. These parts were 3D printed using a Formlab Form2 SLA printer in Durable resin. For precision placement and tolerancing, computer numerical control (CNC) machining was used to drill a 3x3 hole array into the disk. The 30g needles were then press-fit into the disk and a Dremel tool was used to cut off the plastic locking piece of the needle, making the needle flush with the surface of the disk. The disk was placed into the Luer locking component and epoxy resin was poured around the base of the needles. The reservoir has a male Luer lock for connecting to a

25g, blunt-ended needle, polyethylene tubing, and syringe pump, Figure 5.2.

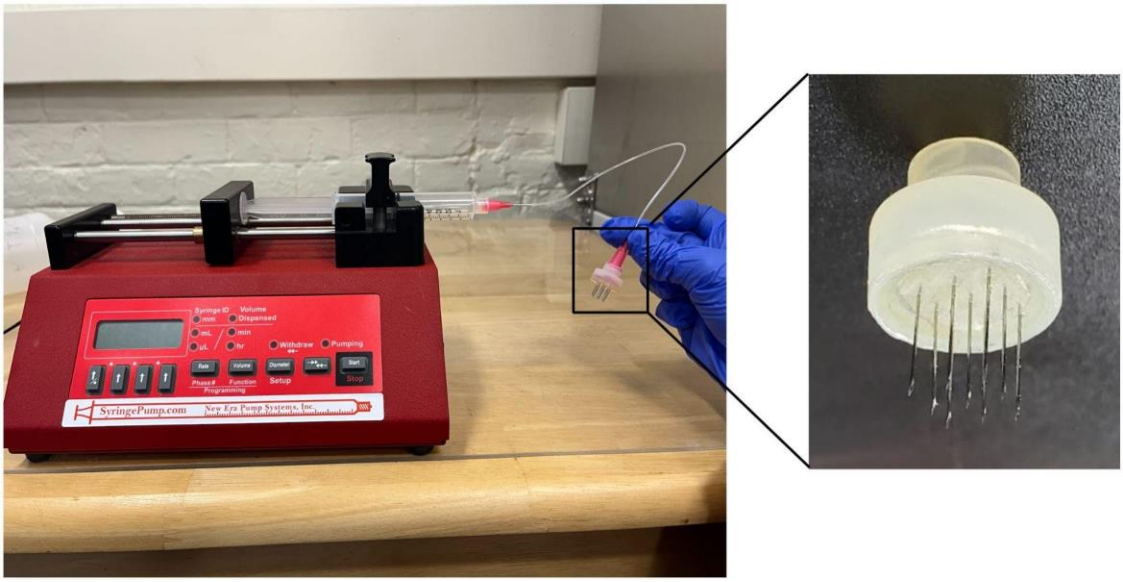

Figure 5. 2: Device Set-up. The device set-up consists of a syringe pump, syringe, 25g needles, polyethylene tubing, and the microneedle reservoir.

5.2 Economics

Our team developed a business canvas model, Figure 5.3, to better understand the business model for our microneedle device. To further expand upon the cost structure of our device, we have included a proposed bill of materials and the estimated cost of these materials, Table 5.1. It costs $780.05 to fabricate one device. Factoring out the syringe pump, which only needs to be purchased one time, the device costs $5.05.

Table 5.1: Business Canvas Model. This model outlines components of our product development, identifies assumptions and risks, and determines potential market obstacles for our device.

<table>
<tr>
<td rowspan="2">Key Partners:
• Shipping companies (for shipping of supplies and our product)
• Medical Device companies/distributors
• Machinists (for fabricating our reservoir)
• Investors</td>
<td>Key Activities:
• Prototyping
• Manufacturing
• Product validation
• Product verification</td>
<td rowspan="2">Value Propositions:
• Ability to recellularize decellularized tissue scaffolds at least one centimeter thick for tissue regeneration.
• Ability to deliver cells via a microneedle device.
• Applicable to a variety of tissue types.</td>
<td>Customer Relationships:
• Ease of use
• Reliable: Failure modes are mitigated
• Feedback from users
• Customer support</td>
<td rowspan="2">Customer Segments:
• Researchers (tissue regeneration, tissue engineering)
• Doctors and surgeons
• Patients with tissue injuries
• Caretakers</td>
</tr>
<tr>
<td>Key Resources:
• Financial support
• Materials (3D print resin, 30g needles, polyethylene tubing, syringe, syringe pump, 25g blunt end needles)
• Engineering and design knowledge
• Patent</td>
<td>Channels:

Medical device distributor</td>
</tr>
<tr>
<td colspan="2">Cost Structure:
• Production costs
• Cost of materials
• Distribution</td>
<td colspan="3">Revenue Streams:
• Recurring payments: The microneedle reservoir component, polyethylene tubing, syringe, and 25g blunt end needles must be purchased new after every use
• One time syringe pump purchase
• Consultation for training and use of the system</td>
</tr>
</table>

Table 5.2: Bill of Materials

Part	Quantity	Cost in Bulk	Cost for One Unit	Purchasing Site
3D Printed Durable Reservoir	1	$1.55/3 reservoirs	$0.52	WPI Rapid Prototyping Lab
3D Printed Dental Disk	1	$1.40/2 disks	$0.70	WPI Rapid Prototyping Lab
30G ½" Sterile Needles	9	$35.58/100 needles	$0.36	Drug Supply Store
JB Weld Professional Grade Epoxy	0.5 mL	$6.98/25 mL	$0.28/mL	Amazon
Syringe Pump	1	$775	$775	New Era Pump Systems Inc.
Sterile Luer Locking Syringe	1	$14.02 per 100 syringes	$0.14	Fisher Scientific
BD Intramedic™ Polyethylene Tubing	0.01207 m	$38.46 per 11 m	$3.50/m	Fisher Scientific
25G Blunt-End Needles	2	$13.60 per 50 needles	$0.27	Harvard Apparatus
Total Cost	**$780.05**			

5.3 Environmental Impact

Our proposed microneedle reservoir system has potential negative environmental impacts. As the device is now, many of the components are single use. The reservoir and disk are currently not reusable, as sterility and cell mixing is a concern when delivering cells to tissue. Therefore, after every use, these reservoirs must be disposed of. Additionally, the needles, syringe, 25G blunt-end needles, and polyethylene tubing attached to the reservoir are also not reusable due to sterility. This could lead to excess plastic and metal waste that could be harmful to the natural environment. However, in the future, methods to sterilize the reservoir, tubing and needles after they have been used could reduce this waste. However, the syringe pump portion of our design can be reused, which eliminates a large amount of waste because the syringe pump is large with many electrical components that could negatively impact the environment if it needed to be disposed of.

5.4 Societal Influence

The proposed microneedle device is expected to have a positive societal influence. Our device would impact a large number of people who have deep tissue injuries. In many of the injuries that cause deep tissue loss, the experience can be extremely traumatizing. This treatment could help give patients the strength and ability to go back to everyday tasks they were able to complete before their injury, as well as speed up the recovery process. Another societal impact this device would have would be for cosmetic applications. Our device could make it easier to treat muscle loss and burn injuries, leading to cosmetic improvements in patients. Additionally, our device could improve the social pressures of being in a hospital and having a different appearance than what is expected in society.

5.5 Political Ramifications

Our novel device is not expected to have a significant political impact. The device could be implemented in many countries with slight modification to the motorized portion. In the short run, this product could lead to less profit in the hospital industry as patients will not be required to pay for multiple surgeries to treat deep tissue injuries. In the long run, our device would positively affect the economy because those being treated with this device would live healthier and happier lives and have the money they would have spent on their surgeries to put into other areas of the economy.

5.6 Ethical Concerns

The ethical concerns of our project arise from the sourcing of materials as well as access in underdeveloped countries. The tissue used for this project was sourced from an animal, which may lead to ethical concerns among different groups of individuals. Our device can be applied to a variety of scaffold types, potentially increasing the ethical concerns of the sourcing of tissue. The cells being used can be sourced from many different places. To ensure the cells are sourced ethically we will follow all applicable standards. Another important concern to address is equal access around the world. The main concern would be lack of electricity to run the syringe pump

in developing countries. Many people in developing countries may not have access to electricity, so they would not be able to use the syringe pump to deliver cells at a precise flow rate. The device could still be accessed without using the set flow rate and manually injecting cells into the tissue; however, tests would need to be conducted to ensure that this method of delivery was as effective Another concern for equal access of our device would be patients' access to appropriate medical centers for treatment. Individuals in other areas of the world may not have access to adequate healthcare, which may limit their ability to use this device. Our device could lead to a better quality of life for patients suffering from deep tissue injuries.

5.7 Health and Safety Issues

The use of needles in our device is the main health and safety issue our device poses. Therefore, this device is meant to be single use and disposed of properly with other medical sharps. Currently, our device is not made of biocompatible material. This could potentially elicit a reaction with human tissue upon contact, as well as with cells flowing through the device. The needles being used are commercial needles that are biocompatible and have a small enough gauge to mitigate tissue damage. Another health concern of this device is plastic leaching. This is due to the material the reservoir is made of. Testing would need to be completed to ensure plastic leaching into the cell suspension does not occur over time. Another health and safety concern would be the cell and tissue sourcing. Standards would need to be followed to ensure this is done correctly and ensure they are safe to use in patients.

5.8 Manufacturability

The device we created could easily be reproduced and enhanced. To reproduce the device, 3D printing and CNC drilling would be needed. Specifically, a Super Mini Mill CNC machine would be necessary, as the drill bit we used was on the micron scale. Additionally, a Dremel would be needed to remove the Luer locks from the 30g needles, but the removal of the plastic Luer lock is a simple process that could be easily repeated. Moving forward, for safety and ease of manufacturability, the device could be created using robotic manufacturing. This would allow the pieces to be produced and assembled in a much quicker and cost effective fashion. Our device can also be easily adapted to different tissue sizes by adjusting the CAD file for the reservoir and manufacturing in the same way.

5.9 Sustainability

The sustainability of our design could be improved. To manufacture our device, large amounts of energy are used for 3D printing as well as CNC drilling. This energy cannot be replaced with other sustainable forms of energy at this moment. To use the device, electricity is used to run the syringe pump, which powers our device. This use of electricity could be evaluated after testing and potentially be removed to increase sustainability. The device is also single use due to health concerns which reduces its sustainability because it necessitates the continuous disposal of metals and plastics.

CHAPTER 6: DESIGN VERIFICATION AND VALIDATION

6.1 Testing Methods

6.1.1 Testing Set-up: Decellularization

While reviewing "Effects of chemical and physical methods on decellularization of murine skeletal muscles" [47], we determined three decellularization protocols (Appendix A) that proved to be successful in varying degrees at eliminating genetic material and cells. These three protocols were performed over the course of 12 days to observe the ability to remove genetic and cellular material based on their varied duration, materials, and technique. Appendix A.1 details the "Freeze" protocol, a twelve-day procedure that utilizes freezing first, then Tris and EDTA as the starting detergent. Appendix A.2 describes the "EDTA + Tris" protocol, a nine-day procedure that utilizes Tris and EDTA as the starting detergent. In Appendix A.3, the "SDS" protocol is outlined, which is a nine-day procedure that utilizes SDS as the starting detergent. Table 6.1 summarizes the three different protocols used. We chose to start the decellularization process with store-bought chicken breast as our samples, mainly due to the easy access and cost-effective nature of this tissue. Based on our revised need statement and the available resources, the chicken samples were sliced into 0.5cm, 1cm, and 2cm cubes. The protocols were performed on the three different sample sizes in triplicate, which validates the results from each procedure.

Table 6.1 Decellularization Protocols. Outlines the main differences between the three protocols used.

Protocol Name	Main Difference	Duration
Freeze	Started in -80℃ freezer for 4 days	12 days
EDTA + Tris	1. EDTA + Tris (2 days) 2. SDS (4 days)	9 days
SDS	1. SDS (4 days) 2. EDTA + tris (2 days)	9 days

Prior to performing decellularization, calculations for chemical volumes were performed and inventory of available materials was taken. For the three different protocols, we used sodium dodecyl sulfate (SDS), Triton X-100, ethylenediaminetetraacetic acid (EDTA), Tris, Penicillin/Streptomycin, and Deionized (DI) water. These reagents each serve a purpose during the decellularization process. SDS is an ionic detergent solution that disrupts the cell membrane and denatures protein in the cells. Triton X-100 is a nonionic detergent that is less aggressive than SDS and is used to lyse the cells of the tissue. After the cells have been disrupted and lysed, EDTA helps to remove them from the ECM, deactivates enzymes, and prevents DNA or RNA degradation. Lastly, Tris increases the permeability of the cell wall to promote cell lysis. Penicillin/Streptomycin prevents bacterial contamination of the tissue. DI water causes the cells to rupture during the first rinse of the tissue because it leads to a hypotonic environment that

causes the cell to burst. The DI water is also used to create diluted solutions with some of the other reagents [67], [68].

6.1.2 Histology and H&E Staining

Histological analysis was performed in the Histology Core at WPI to determine the most effective decellularization procedure. Histology uses microscopy to study the characteristics of tissues and cells. This analysis was performed on three sets of chicken tissue samples from three different decellularization protocols, as well as on control samples. Samples were prepared in three different sizes (0.5 cm^3, 1 cm^3, and 2 cm^3) in triplicate to determine the depth that each protocol could decellularize. The samples were processed and embedded according to the protocol in Appendix B.1. Then, the samples were sectioned according to the protocol in Appendix B.2. Finally, to analyze the samples under a microscope at an objective of 100X, hematoxylin and eosin (H&E) staining was performed according to the protocol in Appendix B.3. Hematoxylin stains the cells' nuclei a purple color. Eosin stains the extracellular matrix and cytoplasm of the cells pink [40].

The protocol determined to be the most effective in cell removal, the SDS protocol, was used again to ensure that cells could be removed from bovine skeletal muscle samples prior to device testing. This analysis was performed on three 1cm^3 bovine muscle samples. H&E staining was conducted and the decellularized samples were compared to control samples for the presence of cells. After determining that the SDS protocol completely removed cells from bovine muscle samples, the samples were decellularized and cells were delivered to samples using our microneedle device. H&E staining was performed to determine if cells were present after recellularization with our microneedle device.

6.1.3 Picrosirius Red/Fast Green Staining

Picrosirius Red/Fast Green staining was performed in the Histology Core at WPI as well to determine if the optimal decellularization procedure preserved the matrix structure of the tissue samples. Picrosirius Red/Fast Green staining was performed according to the protocol in Appendix B. 4. The Picrosirius Red stains collagenous components of tissue red. The Fast Green counterstain stains non-collagen proteins green [69]. This analysis was performed on three non-decellularized control samples and three decellularized samples of 1cm^3 bovine muscle tissue. The samples were processed and embedded according to the protocol in Appendix B.1. Then, the samples were sectioned according to the protocol in Appendix B.2. The samples were imaged under a microscope at an objective of 100X.

6.1.4 Cell Viability

Cell viability on the decellularized bovine skeletal tissue was tested using the protocol in Appendix C.1. Cell viability of the MDA-MB-231/GFP/Blasticidine cell line was examined to ensure that our scaffolds would not kill cells. This cell line was used because it contains green fluorescent protein (GFP). The GFP is only visible in viable cells, which made it easier to determine if the cells lived on our scaffolds. Cells were seeded at varying densities to determine

an optimal density for delivery of cells to the bovine skeletal muscle scaffolds. Each cell density was tested on three separate decellularized tissue scaffolds (n=3).

6.1.5 Long-Term Storage Viability Testing

To determine the ability of our decellularized bovine skeletal muscle scaffolds to be stored long-term and still support viable cells, samples were frozen and stored at -20°C, -80°C, and in liquid nitrogen for over 1 week. Long-term storage of the decellularized scaffolds is important to examine because the ability to store and transport these scaffolds for an extended period of time would be beneficial for the translation to the medical device market or to clinicians. The protocol in Appendix C.2 was followed to examine cell viability on the scaffolds after long-term storage at each of these conditions. Three decellularized tissue scaffolds were tested for each long-term storage condition (n=3).

6.1.6 Scanning Electron Microscopy

Scanning electron microscopy (SEM) was performed to evaluate the 3D structure of both control and decellularized bovine skeletal muscle. SEM uses an electron beam to interact with the surface of the tissue to collect information related to surface topography, crystalline structure, composition, and electrical behavior [28], [46]. Specifically, the Phenom G1 Scanning Electron Microscope was used in the User-Friendly Characterization Laboratory at WPI. This microscope is capable of a 120X to 24,000X objective, with the 120X to 10,000X range being the most effective. The samples were prepared for SEM and imaged according to the protocol in Appendix C.3. Average pore size in both control and decellularized samples were determined using ImageJ and compared to assess if the decellularization protocol altered the structure of the samples.

6.1.8 Device Leak Testing

To ensure that our device would not leak during cell delivery, our team performed a leak test following the protocol in Appendix C.5. Briefly, our microneedle device was attached to an adaptor connected to the rest of the syringe pump system, and the device and attached adaptor were submerged as air was passed through, as shown in the schematic in Figure 6.1. Visual inspection was used to determine if there was air leakage occurring anywhere.

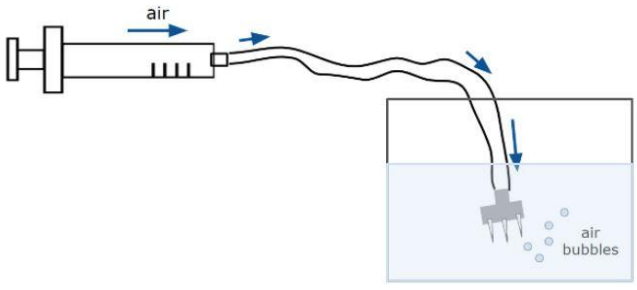

Figure 6.1: Air Leak Test Set-up.

6.1.9 Volume and Cell Retention Testing

We used volume and cell retention testing to determine the volume of liquid and the number of cells that would leak out of the tissue scaffolds after delivery with our microneedle device. This testing helped to determine if cells were retained in the tissue scaffold after delivery. To conduct the volume and cell retention testing, we followed the protocol found in Appendix C.4. A cell suspension at a concentration of 10 million cells/mL was delivered to three different decellularized bovine skeletal muscle scaffolds. The change in tissue weight, the volume remaining in the well plate, and the number of cells counted in the well plate were recorded for analysis. The number of cells remaining in the well was then used to calculate the percentage of cells retained by the tissue scaffold using the following equations:

$$\frac{Total\ \#\ of\ cells\ in\ well}{(\frac{10\ million\ cells}{mL} * volume\ delivered\ in\ mL)} * 100 = \%\ of\ cells\ leaked \quad \text{(Eq 1)}$$

$$100\% - \%\ of\ cells\ leaked = \%\ of\ cells\ retained\ in\ scaffold \quad \text{(Eq 2)}$$

6.1.10 Flow Rate and Cell Delivery Testing

To assess the optimal flow rate to deliver cell suspension to our decellularized tissue scaffolds that would allow the cells adequate time to attach to the scaffold, our team performed a flow rate and cell delivery test following the protocol in Appendix C.6. Briefly, our team used our microneedle reservoir system to test three flow rates and delivered 1 mL of cell suspension to the decellularized tissue scaffolds. These flow rates were based on values from previous literature and our observations [70]. A volume of 1 mL was chosen for delivery because that is the maximum possible volume that our 1 cm^3 scaffolds could hold if they were completely empty. A cell density of 1 million cells/mL was delivered in 1 mL of media, so 1 million cells were delivered to each scaffold. The MDA-MB-231/GFP/Blasticidine cell line was used for this test. This cell density was selected because in the cell viability tests on our decellularized tissue scaffolds, 200,000 cells were delivered to the scaffolds and some loss occurred. Therefore, we wanted to ensure that enough cells were being delivered within the scaffolds. Following cell delivery, the volume of leaked media and the number of cells present in that media were measured, as they were in the volume and cell retention test (see Appendix C.5). Then H&E staining (see Appendix B.3) was performed to confirm if cells were present in the scaffold after 3 days in culture. Three decellularized tissue scaffolds were used for each flow rate to test cell delivery (n=3).

6.2 Results

6.2.1 Histology and H&E Staining

6.2.1.1 Decellularization Protocol Optimization

Following histological sectioning and H&E staining of decellularized chicken tissue samples, the chicken tissue samples were imaged and compared among each other and to the control to determine the optimal decellularization protocol to use. Figure 6.2 shows the chicken

tissue control samples after H&E staining. Each size sample has purple nuclei present, indicating that the control samples contained cells.

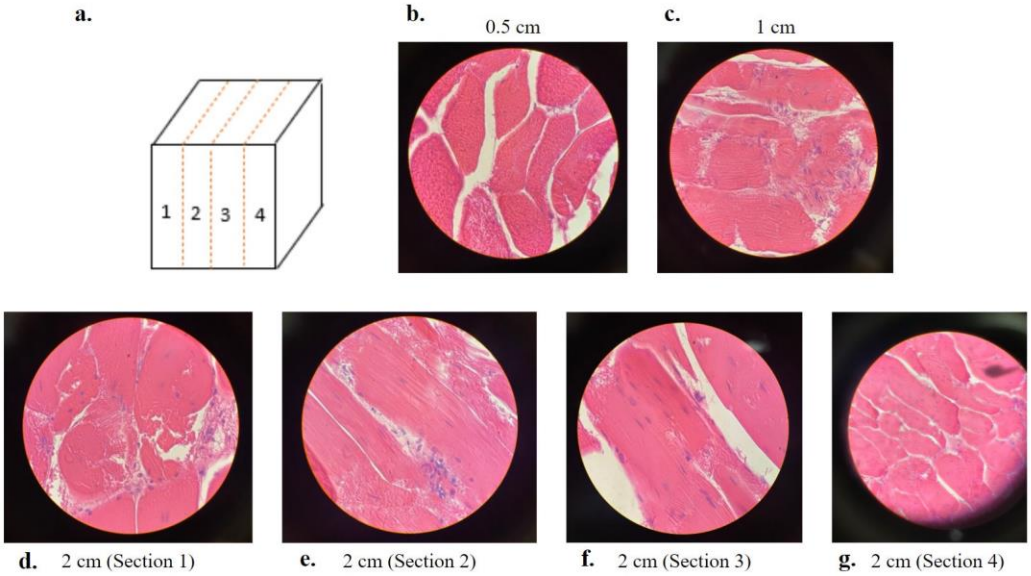

Figure 6.2 H&E Staining of Chicken Tissue Control Samples. The 2cm^3 control samples were sectioned (a) and stained in four parts (d-g). The 0.5cm^3 (b) and the 1cm^3 (c) samples were stained as a whole piece. Pink stain represents cytoplasm and purple stain represents cell nuclei.

Figure 6.3 shows the histological sections of chicken breast samples decellularized with the Freeze protocol (see Appendix A.1) from "sample A" chicken breast pieces. Cytoplasmic components were present in all samples. The presence of nuclei was reduced compared to the control samples and samples decellularized with the EDTA + Tris Protocol. However, some nuclei were still detected, as shown in Figure 6.3 d and f. Additionally, the presence of nuclei can be seen in the histological sections of sample B, shown in Appendix D.

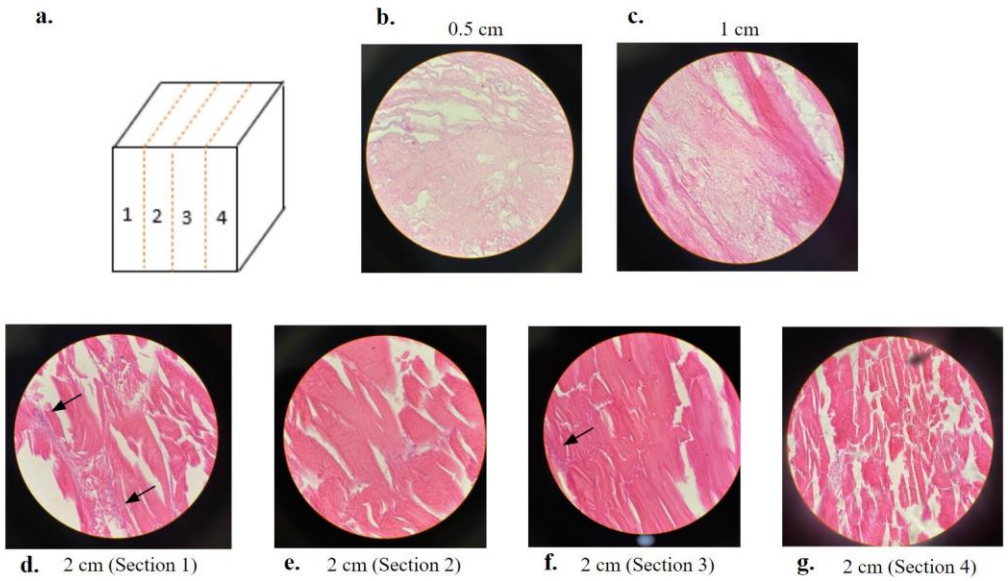

Figure 6.3 H&E Staining of Decellularized Chicken Tissue from the Freeze Protocol. Images were selected from one of three sets of samples as representative results (Sample A). The 2cm^3 control samples were sectioned (a) and stained in four parts (d-g) (Section 4 sectioned at 10µm instead of 5µm). The 0.5cm^3 (b) and the 1cm^3 (c) samples were stained as a whole piece. Pink stain represents cytoplasm and purple stain represents cell nuclei. Black dots are debris on the microscope. Black arrows indicate cells.

Histological sections of chicken breast samples from "sample A" pieces following decellularization with the EDTA + Tris protocol (see Appendix A.2) can be seen in Figure 6.4. Each sample shows the presence of cytoplasmic components. Additionally, the images show that some cells remain in the chicken breast following decellularization with the EDTA + Tris protocol, indicated by the purple stain present in the samples. Particularly, in Figure 6.4 c, d, and f, nuclei were detected. While there were nuclei detected, there was a reduced number of nuclei compared to the control samples. Based on these findings, the EDTA + Tris protocol was not able to completely decellularize the tissue. Further evidence of the presence of nuclei can be seen in the histological sections of samples B and C, found in Appendix D.

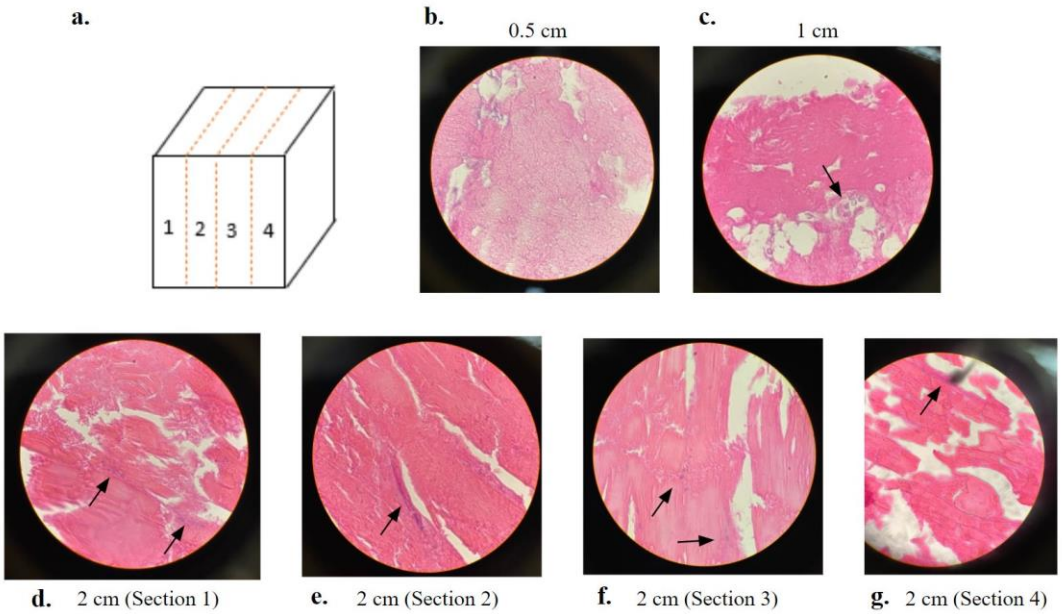

Figure 6.4 H&E Staining of Decellularized Chicken Tissue from the EDTA + Tris Protocol. Images were selected from one of three sets of samples as representative results (Sample A). The 2cm^3 control samples were sectioned (a) and stained in four parts (d-g) (Section 4 sectioned at 10µm instead of 5µm). The 0.5cm^3 (b) and the 1cm^3 (c) samples were stained as a whole piece. Pink stain represents cytoplasm and purple stain represents cell nuclei. Black dots are debris on the microscope. Black arrows indicate cells.

Figure 6.5 shows the chicken breast samples that were decellularized using the SDS protocol (see Appendix A.3) from "sample A" chicken breast pieces. Each sample was properly stained, as cytoplasmic components were detected in the decellularized chicken samples. The lack of purple stain in each size sample indicates that the chicken samples were completely decellularized using the SDS protocol when compared with the control samples. These results indicate that the SDS protocol can decellularize tissue up to a depth of 2 cm. A lack of nuclei was also seen in samples B and C chicken breast, refer to Appendix D, and verify that the SDS protocol was able to decellularize chicken breast up to a depth of 2 cm.

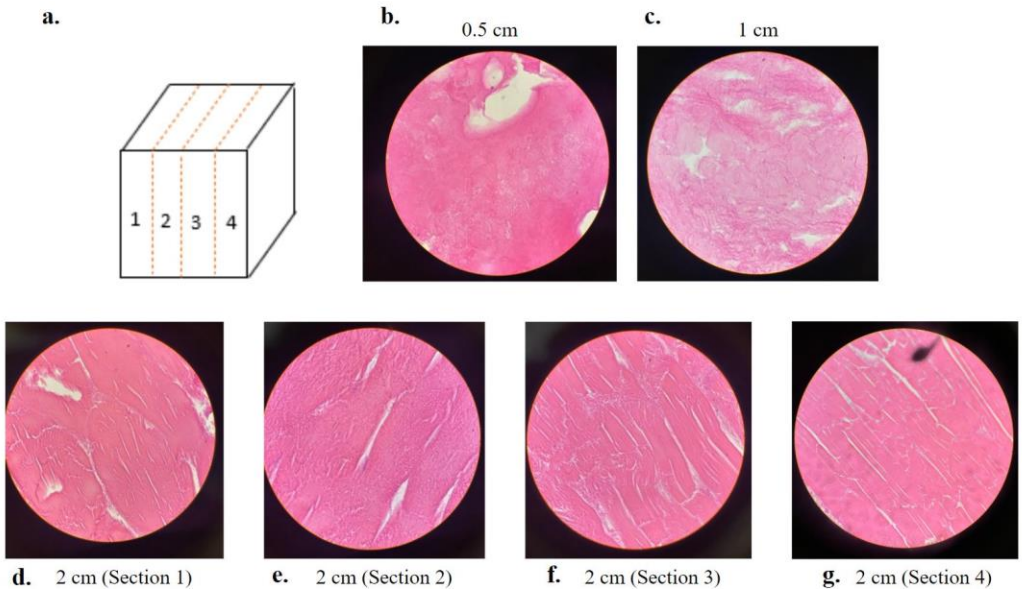

Figure 6.5 H&E Staining of Decellularized Chicken Tissue from the SDS Protocol. Images were selected from one of three sets of samples as representative results (Sample A). The 2cm^3 control samples were sectioned (a) and stained in four parts (d-g). The 0.5cm^3 (b) and the 1cm^3 (c) samples were stained as a whole piece. Pink stain represents cytoplasm and purple stain represents cell nuclei. Black dots are debris on the microscope.

The initial decellularization protocol optimization indicates that the SDS protocol is the most effective in decellularizing tissue samples up to 2 cm^3 when compared to the control samples and the EDTA + Tris or the Freeze protocols. Additionally, after the decellularization process, our team discovered that the 0.5 cm^3 samples were too small to decellularize, leaving only small pieces of tissue for histological analysis. Therefore, for device testing, decellularization using the SDS protocol was conducted and 1 cm^3 samples were used.

6.2.1.1 Decellularization and Recellularization of Bovine Muscle Tissue

Decellularized and control samples of bovine skeletal muscle were stained and imaged as seen in Figure 6.6. Three decellularized samples were compared to the three control samples to determine if the SDS protocol could remove cells from bovine skeletal muscle. All control samples had an abundance of cells present, indicated by the purple nuclei in the images. In comparison, decellularized samples had no nuclei present. These images indicate that the SDS protocol was able to remove cells from bovine skeletal muscle to the same degree as in chicken tissue.

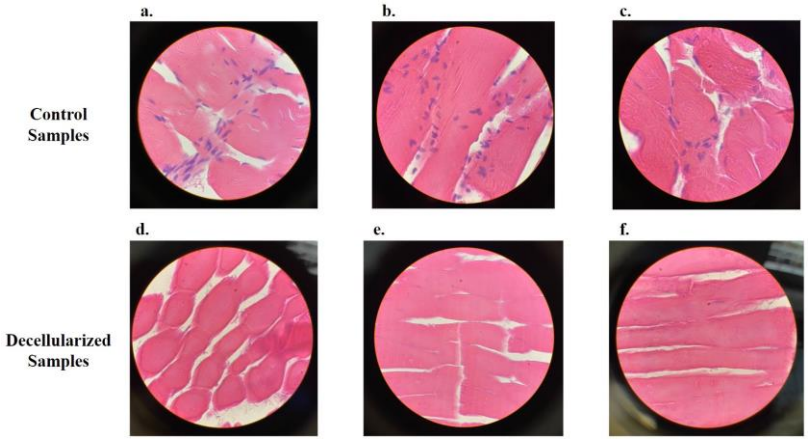

Figure 6.6 H&E Staining of Decellularized Bovine Muscle Tissue. Samples are 1cm^3. Control samples (a-c) did not undergo decellularization. Decellularized samples (d-f) were decellularized using the SDS protocol. Pink stain represents cytoplasm and purple stain represents cell nuclei.

6.2.2 Picrosirius Red/Fast Green Staining

Following histological sectioning and Picrosirius Red/Fast Green staining of decellularized bovine muscle tissue, the samples were imaged and compared to the controls to determine if the SDS protocol preserved the matrix structure of the samples. Figure 6.7 shows the control, non-decellularized samples, as well as the samples decellularized with the SDS protocol. Both control and decellularized samples have similar amounts of red and green stains present. Decellularized sample 1 shows a slightly smaller amount of red stain present, indicating a slightly lower collagen content. However, this could be attributed to the sample itself, and not the decellularization procedure. These images show that the collagenous and non-collagenous matrix proteins were preserved through the decellularization process.

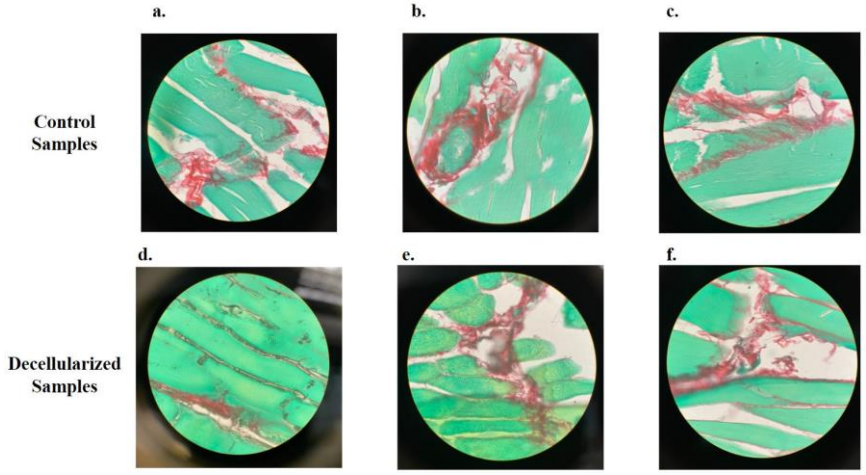

Figure 6.7 Picrosirius Red/Fast Green Staining of Control and Decellularized Bovine Skeletal Muscle. 1cm^3 skeletal muscle tissue blocks were used. Control samples (a-c) did not undergo decellularization. Decellularized samples (d-f) were decellularized using the SDS protocol. Red stain represents collagen and green stain represents counterstain for non-collagenous portions.

6.2.3 Scanning Electron Microscopy

Following sample preparation, decellularized and control bovine skeletal muscle was imaged with SEM to determine if the structure of the ECM was preserved using the SDS decellularization protocol. Figure 6.8 shows control and decellularized bovine skeletal muscle samples at three magnifications. Fibrous structures are seen in both control and decellularized SEM images. As magnification increases, smaller pores are visible in these fibers. Visually, the decellularized control samples appear to have larger gaps between fibers, which could be attributed to cell loss. Table 6.2 compares the average pore area between control and decellularized bovine skeletal muscle samples. The decellularized muscle tissue has a larger maximum pore size, which could be due to the cell loss previously mentioned.

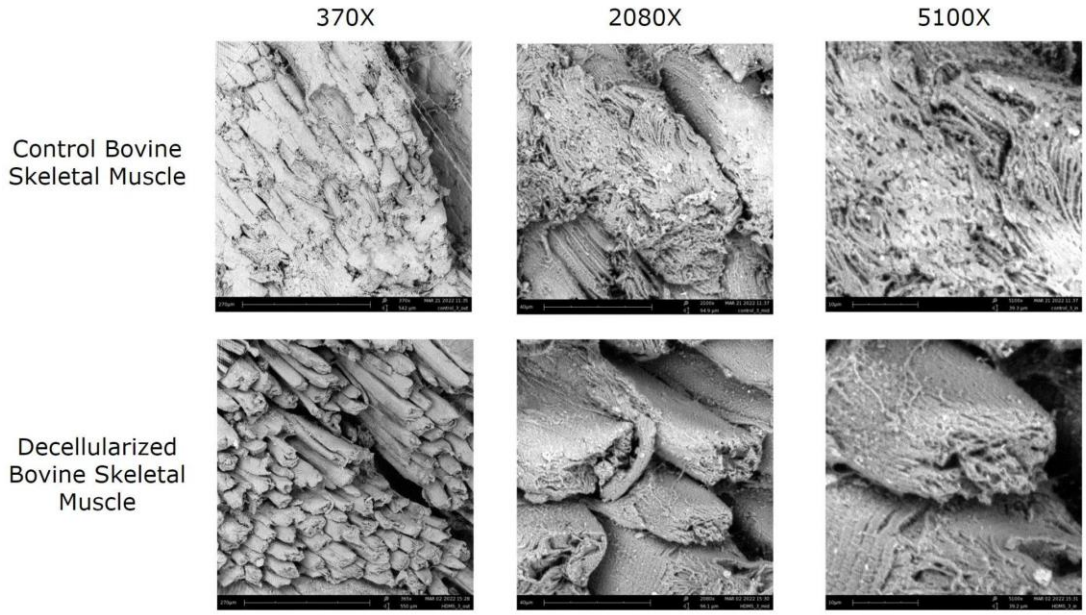

Figure 6.8: SEM Imaging of Control and Decellularized Bovine Skeletal Muscle. 370X scale bar: 270 µm, 2080X scale bar: 40 µm, 5100X scale bar: 10 µm.

Table 6.2 Maximum and Minimum Pore Area of Decellularized and Control Bovine Skeletal Muscle. Calculated using particle analyzer on SEM images in ImageJ.

	Minimum Pore Size	**Maximum Pore Size**
Control Bovine Skeletal Muscle	0.0014 μm^2	1429 μm^2
Decellularized Bovine Skeletal Muscle	0.0015 μm^2	5130 μm^2

6.2.4 Cell Viability

Fluorescence microscopy was used to image decellularized bovine skeletal muscle samples seeded with MDA-MB-231/GFP/Blasticidine cells, seen in the representative images in Figure 6.9. Green signal indicates viable cells, which are seen on all samples. Scaffolds seeded with 20,000 cells show a minimal amount of viable cells, indicating that this density is not

adequate for delivery. Samples seeded with a higher cell density show an increased viability of cells at days 3 and 7. However, the cells did not take on the elongated morphology that they exhibited on tissue culture plastic. Instead, the cells are smaller and rounded. Additionally, the number of viable cells appeared to decrease between days 3 and 7, which could be due to flipping of the samples; however, it may also be due to not being able to image the same area of the tissue every time. The difference in morphology and the reduced amount of GFP expressed by the cells indicate how the cells act on our decellularized tissue scaffolds compared to tissue culture plastic.

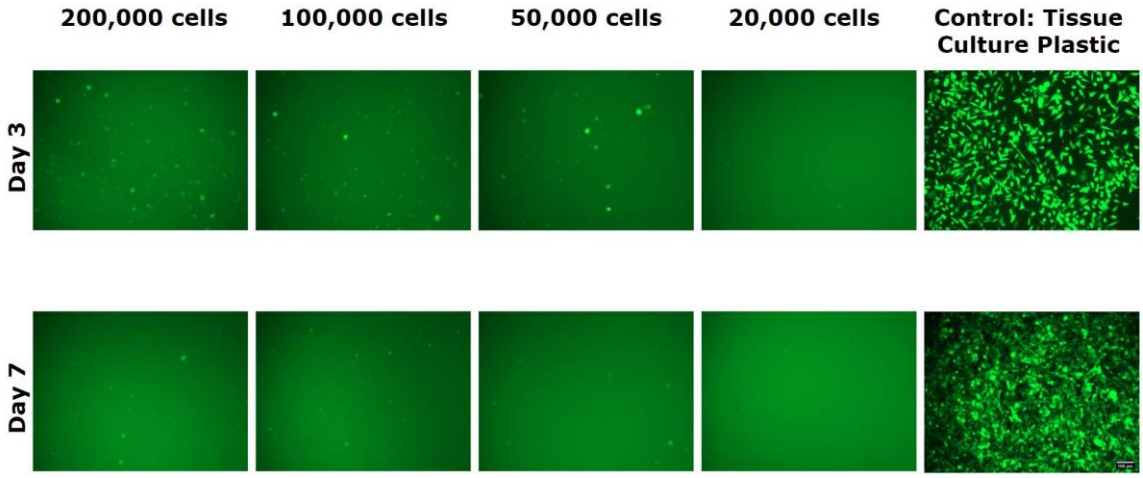

Figure 6.9: Fluorescence Microscopy of MDA-MB-231/GFP/Blasticidine cells on Bovine Skeletal Muscle. Samples were flipped before imaging and flipped back after imaging. Objective: 10X, scale bar (white): 100µm.

6.2.5 Long-Term Storage Viability Testing

To image MDA-MB-231/GFP/Blasticidine cells seeded on decellularized bovine skeletal muscles stored in liquid nitrogen, -80℃, and -20℃, fluorescence microscopy was used. Representative images of cells on these scaffolds are shown in Figure 6.10. Cells were viable on the decellularized tissue at days 3 and 7 after long-term storage at all conditions. Viable cells could be seen in different planes of focus, due to the topography of the decellularized tissue scaffolds. The viable cells exhibited an altered morphology on the decellularized bovine skeletal muscle stored for an extended period of time compared to the tissue culture plastic control as the cells were rounded and appeared smaller. Increased cell viability was observed on the liquid nitrogen samples, indicating that liquid nitrogen may be the best storage method for the decellularized tissue scaffolds. Autofluorescence was difficult to overcome during imaging, which may have impacted our ability to view cells on the scaffolds.

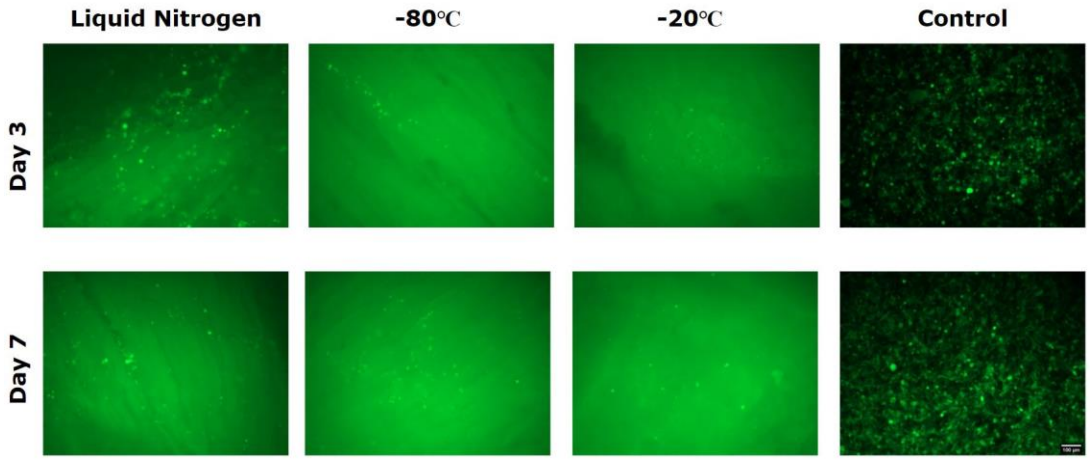

Figure 6.10: Fluorescence Microscopy of MDA-MB-231/GFP/Blasticidine cells on Bovine Skeletal Muscle Stored Long-Term. Samples were flipped before imaging and flipped back after imaging. Objective: 100X, scale bar (white): 100μm.

6.2.6 Device Leak Testing

Visual inspection of our microneedle device submerged in water with air passed through the assembly showed no bubbles occurring anywhere other than the needle tips. This indicated to our team that there are no leaks in our device. Additionally, this showed us that our microneedle device allows the passage of air or fluid through the device.

6.2.7 Volume and Cell Retention Testing

Table 6.3 contains the results from the volume and cell retention test, in which 10 million cells/mL were delivered in a 250 μL droplet to 1cm thick decellularized bovine muscle tissue. After delivery of cells with our microneedle device, the tissue weighed less and the volume leaked from samples 1 and 3 was more than the volume of cell suspension delivered to the tissue. This may be attributed to the fact that DPBS(-) that the scaffolds were stored in may have been trapped within the tissue, and the delivery of cells may have pushed this excess fluid out of the tissue. The percentage of cells retained indicates that although media leaked from the scaffolds during delivery, a majority of the cells were retained within the scaffolds.

Table 6.3: Volume and Retention Test Results. Weight of the tissue sample before and after delivery, volume leaked, cell count in the leaked volume, % of cells leaked, and % of cells retained were observed.

Sample #	Weight Before (g)	Weight After (g)	Volume leaked (µL)	Cell count	% of Cells Leaked	% of Cells Retained
1	1.84 ± 0.04	1.65 ± 0.004	288	319,000 cells	12.76%	87.24%
2	1.39 ± 0.02	1.18 ± 0.002	92	23,276 cells	0.93%	99.07%
3	2.46 ± 0.04	2.13 ± 0.002	280	226,000 cells	9.04%	90.96%

6.2.8 Flow Rate and Cell Delivery Testing

Table 6.4 outlines the results immediately after 1 million cells/mL were delivered to the decellularized tissue scaffolds in a volume of 1 mL. While all of the media that was delivered appeared to leak from each of the scaffolds, after performing a cell count from samples of the leaked media, it appears that over 80% of cells were retained for all three flow rates. According to the percentage of cells retained, a flow rate of 0.6 mL/min appears to retain the most cells. H&E staining confirmed the presence of cells in one centimeter thick tissue scaffolds, Figure 6.13. Scaffolds injected at a flow rate of 0.6 mL/min showed more consistency compared to a flow rate of 1.2 mL/min and 1.8 mL/min.

Table 6.4: Volume and retention of cells after delivery at different flow rates.

Flow Rate	Volume leaked	Cell count	% of Cells Leaked	% of Cells Retained
0.6 mL/min	1 mL	12,500 cells	1.25%	98.75%
1.2 mL/min	1 mL	107,500 cells	10.75%	89.25%
1.8 mL/min	1.2 mL	177,000 cells	17.70%	82.30%

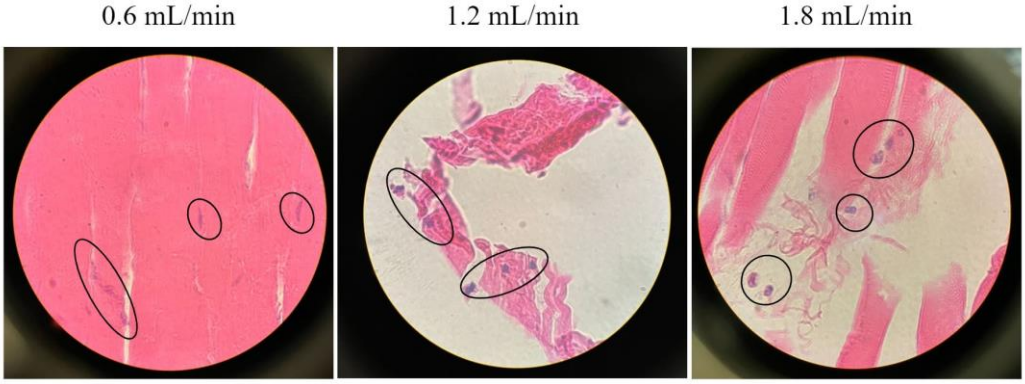

Figure 6.13 H&E Staining of Decellularized Tissue Scaffolds with Cells Delivered. Images are shown in the center of the scaffolds. The black circles indicate the nuclei.

CHAPTER 7: DISCUSSION

Optimization of the decellularization of tissue allowed our team to determine the protocol that removed the most cells from tissue samples. This was important for future validation experiments in which we delivered cells via our microneedle device to decellularized tissue. The SDS protocol was determined the most optimal protocol for decellularizing tissue derived from chicken compared to the EDTA + Tris and Freeze protocols, and was able to completely remove cells from bovine skeletal muscle for use in device testing. Additionally, based on the Picrosirius Red/Fast Green staining, the SDS protocol did not destroy the collagenous and non-collagenous proteins in the matrix of bovine skeletal muscle. This was confirmed with SEM imaging, which showed intact muscle fibers in both control and decellularized bovine skeletal muscle samples. However, the decellularized muscle samples had a larger maximum pore size of 5130 μm^2, compared to the control muscle samples that had a maximum pore size of 1429 μm^2. This could be due to loss of cellular components in the decellularized muscle samples. Miranda et al. (2021) conducted a decellularization study on murine muscle tissue showing similar results, with the SDS protocol being optimal for cell removal and preservation of matrix structure [47].

Assessment of cell viability on top of the decellularized tissue scaffolds indicated that MDA-MB-231/GFP/Blasticidine cells are viable on the decellularized tissue scaffolds, as only viable cells express the fluoresce. However, the cell morphology is smaller and rounder compared to cells on tissue culture plastic. The same viability and morphology were observed when cells were seeded on the decellularized tissue scaffolds stored at different temperatures in the long term. These results show that decellularized tissue scaffolds support viable cells. While there appears to be cellular loss between days 3 and 7 of culture, this can be attributed to not being able to image the exact same area on the tissue over multiple days, as the number of cells varies in different areas. Additionally, the results demonstrate that liquid nitrogen is the optimal long-term storage condition for the decellularized tissue scaffolds. This shows the utility of the scaffolds because they can be stored for use at a later date and still maintain viable cells. A limitation of the viability testing was that we could not overcome the autofluorescence during imaging, which made it more difficult to visualize the viable cells present on the scaffolds.

Leak testing demonstrated the ability of our microneedle reservoir to hold cell suspension prior to delivery and allow the passage of fluid via the needle tips. This was necessary for the utility of our device. Delivery of cells into one centimeter thick decellularized bovine skeletal muscle with our device validated that cells could be retained by our scaffold, with each sample retaining over 85% of the cells delivered. Following the initial cell retention testing, the delivery of cells at three controlled rates into one centimeter thick decellularized tissue scaffolds with our device confirmed that over 80% of cells were retained for all flow rates, with over 90% cell retention in samples with cells delivered at 0.6 mL/min. Additionally, histological analysis after 3 days of culture confirmed the presence of cells in the scaffolds. Scaffolds injected at a flow rate of 0.6 mL/min showed more consistency compared to a flow rate of 1.2 mL/min and 1.8 mL/min.

These results from verification and validation testing confirm that our microneedle

reservoir device met the design objectives and constraints outlined by our team at the beginning of this project. The results indicate that the device is able to penetrate and deliver viable cells to one centimeter thick decellularized tissue scaffolds. Prior to delivery, the microneedle reservoir system was able to temporarily hold cells at room temperature for a short period of time prior to their release. A range of volumes can be delivered to the tissue via the device based on syringe selection and size of the tissue scaffolds. Cell suspensions can be delivered at precise volumes and controlled flow rates as well to allow for improved cell retention. The device was able to be fabricated with 30g needles, which have an outer diameter of 312μm, and therefore meets the performance specification of having a needle diameter of 350μm. The device was low cost, as multiple microneedle devices were able to be fabricated within the budget of $1000.

The results show proof-of-concept for a microneedle reservoir system capable of delivering cells to one centimeter thick decellularized tissue scaffolds. This is deeper than commercial microneedles, which can only reach a maximum depth of 200 microns [27]. Additionally, this technology would offer favorable treatments over the current deep tissue injury treatment options. This design would offer faster tissue regeneration due to the ability to seed the scaffold with appropriate cells prior to implantation.

CHAPTER 8: CONCLUSIONS AND RECOMMENDATIONS

The fabricated microneedle and cell reservoir system is capable of delivering viable cells to one centimeter thick decellularized tissue scaffolds. The device can temporarily store cell suspension of various volumes at room temperature before injection based on syringe selection and the size of the scaffold. With an optimal flow rate of 0.6 mL/min, injection of cells into decellularized tissue scaffolds using the device resulted in 90% cell retention and verified recellularization. The use of 30g microneedles for successful recellularization of tissue scaffolds is a novel approach for substantial tissue regeneration. With the use of this device, recellularized tissue scaffolds could offer an advantageous alternative to autografts, allografts, bioengineered skin substitutes, and xenografts. Successful recellularization of tissue scaffolds overcomes the inability to regenerate functional tissue following injury and insufficient natural recellularization into the center of implanted tissue scaffolds.

The device was designed for versatility and adaptability. Future iterations of the device should increase the depth of delivery, improve usability, and be completely biocompatible. For proof of concept, initial prototypes were fabricated with 1.3 centimeter microneedles. The fabrication components of the device disk and epoxy minimize deflection of the needles, and additional guide components can be added to compensate for the decreasing aspect ratio of longer needles for a straight trajectory into tissue. Additionally, a smaller bore size for the microneedles to minimize tissue damage, and a dense needle array for uniform cell distribution in the scaffold should be pursued. To achieve this goal, professional-grade metallic nano 3D printing should be considered. Accessories can also be developed to customize the device for the setting. If the device is being used manually, grips or extensions can be used to help with usability. The device can also easily be incorporated into a robotic system for automated usage.

Continued functional testing can be conducted to improve the performance of the device using viscosity testing and assays. Performance specifications will need to be developed to determine the minimum number of cells delivered and the percentage of proliferating cells for effective tissue regeneration. The viscosity of the injected media should also be optimized to enhance cell attachment and proliferation in the scaffold while minimizing leakage during injection. Further research should be conducted to determine an appropriate extracellular matrix protein for the media to allow for sufficient cell adhesion to the scaffold. The simplicity of the device allows for continued improvement and versatility.

References

[1] R. Stone II *et al.*, "Advancements in Regenerative Strategies Through the Continuum of Burn Care," *Front. Pharmacol.*, vol. 0, 2018, doi: 10.3389/fphar.2018.00672.

[2] L. DeSanti, "Pathophysiology and Current Management of Burn Injury," *Adv. Skin Wound Care*, vol. 18, no. 6, pp. 323–332, Aug. 2005.

[3] M. G. Jeschke, M. E. van Baar, M. A. Choudhry, K. K. Chung, N. S. Gibran, and S. Logsetty, "Burn injury," *Nat. Rev. Dis. Primer*, vol. 6, no. 1, p. 11, 2020, doi: 10.1038/s41572-020-0145-5.

[4] S. Hettiaratchy and P. Dziewulski, "Pathophysiology and types of burns," *BMJ*, vol. 328, no. 7453, pp. 1427–1429, Jun. 2004.

[5] A. Shpichka *et al.*, "Skin tissue regeneration for burn injury," *Stem Cell Res. Ther.*, vol. 10, no. 1, p. 94, Mar. 2019, doi: 10.1186/s13287-019-1203-3.

[6] G. D. Mulbauer and H. W. T. Matthew, "Biomimetic Scaffolds in Skeletal Muscle Regeneration," *Discoveries*, vol. 7, no. 1, p. e90, doi: 10.15190/d.2019.3.

[7] S. Baiguera, C. Del Gaudio, P. Di Nardo, V. Manzari, F. Carotenuto, and L. Teodori, "3D Printing Decellularized Extracellular Matrix to Design Biomimetic Scaffolds for Skeletal Muscle Tissue Engineering," *BioMed Res. Int.*, vol. 2020, p. e2689701, Nov. 2020, doi: 10.1155/2020/2689701.

[8] C. McCuller, R. Jessu, and A. L. Callahan, "Physiology, Skeletal Muscle," in *StatPearls*, Treasure Island (FL): StatPearls Publishing, 2021. Accessed: Aug. 30, 2021. [Online]. Available: http://www.ncbi.nlm.nih.gov/books/NBK537139/

[9] L. M. Biga *et al.*, "10.2 Skeletal Muscle," 2019, Accessed: Aug. 30, 2021. [Online]. Available: https://open.oregonstate.education/aandp/chapter/10-2-skeletal-muscle/

[10] T. Sarrafian, S. Bodine, B. Murphy, K. Grayson, and S. Stover, "Extracellular matrix scaffolds for treatment of large volume muscle injuries," *Am. Coll. Vet. Surg.*, Nov. 2017, doi: 10.1111/vsu.12787.

[11] B. Langridge, M. Griffin, and P. E. Butler, "Regenerative medicine for skeletal muscle loss: a review of current tissue engineering approaches," *J. Mater. Sci. Mater. Med.*, vol. 32, no. 1, p. 15, Jan. 2021, doi: 10.1007/s10856-020-06476-5.

[12] S. Testa *et al.*, "The War after War: Volumetric Muscle Loss Incidence, Implication, Current Therapies and Emerging Reconstructive Strategies, a Comprehensive Review," *Biomedicines*, vol. 9, no. 5, Art. no. 5, May 2021, doi: 10.3390/biomedicines9050564.

[13] "Volumetric Muscle Loss (VML) Repair Following Extremity Trauma - MTEC." https://www.mtec-sc.org/mtec-current-projects/volumetric-muscle-loss-vml-repair-following-extremity-trauma/ (accessed Sep. 06, 2021).

[14] A. M. Basten, C. J. Raymond-Pope, K. A. Dalske, J. A. Call, and S. M. Greising, "Metabolic and Contractile Pathophysiology Following Volumetric Muscle Loss Injury," *FASEB J.*, vol. 34, no. S1, pp. 1–1, 2020, doi: 10.1096/fasebj.2020.34.s1.03094.

[15] A. Porzionato, E. Stocco, S. Barbon, F. Grandi, V. Macchi, and R. De Caro, "Tissue-Engineered Grafts from Human Decellularized Extracellular Matrices: A Systematic Review and Future Perspectives," *Int. J. Mol. Sci.*, vol. 19, no. 12, p. 4117, Dec. 2018, doi: 10.3390/ijms19124117.

[16] "Treatment with Epicel." https://www.epicel.com/treatment-with-epicel.html# (accessed Aug. 29, 2021).

[17] "Benefits and associated risks of using allograft, autograft and synthetic bone fusion material for patients and service providers - A Systematic Review," *JBI Evid. Synth.*, vol. 8, no. 8, pp. 1–13, 2010, doi: 10.11124/jbisrir-2010-851.

[18] Organogenesis Inc., "Dermagraft Human fibroblast-dervied dermal substitute: Directions for Use." [Online]. Available: https://dermagraft.com/pdf/Dermagraft-Directions-for-Use.pdf

[19] E. García-Gareta, Y. Abduldaiem, P. Sawadkar, C. Kyriakidis, F. Lali, and K. V. Greco, "Decellularised scaffolds: just a framework? Current knowledge and future directions," *J. Tissue Eng.*, vol. 11, p. 2041731420942903, Jan. 2020, doi: 10.1177/2041731420942903.

[20] Organogenesis Inc., “Apligraf Package Insert.” [Online]. Available: https://apligraf.com/pdf/Apligraf-Package-Insert.pdf
[21] Integra, “Integra Dermal Regeneration Template.” [Online]. Available: https://www.integralife.com/file/general/1453795605-1.pdf
[22] A. M. Harmon, S. M. Kladakis, and J. Hwang, “Viable Tissue Repair Implants and Methods of Use,” US 8 641 775 B2, Feb. 04, 2014 [Online]. Available: https://patentimages.storage.googleapis.com/b0/2d/dc/1ba559990af602/US8641775.pdf
[23] T. K. Rajab, T. J. O’Malley, and V. Tchantchaleishvili, “Decellularized scaffolds for tissue engineering: Current status and future perspective,” *Artif. Organs*, vol. 44, no. 10, pp. 1031–1043, 2020, doi: 10.1111/aor.13701.
[24] C. Bilodeau, O. Goltsis, I. M. Rogers, and M. Post, “Limitations of recellularized biological scaffolds for human transplantation,” *J. Tissue Eng. Regen. Med.*, vol. 14, no. 3, pp. 521–538, 2020, doi: 10.1002/term.3004.
[25] S. Ambady, “Microneedle Assisted Delivery of Cells to Decellularized Tissue Project Description,” 2021.
[26] S. R. Dabbagh, M. R. Sarabi, R. Rahbarghazi, E. Sokullu, A. K. Yetisen, and S. Tasoglu, “3D-printed microneedles in biomedical applications,” *iScience*, vol. 24, no. 1, p. 102012, Jan. 2021, doi: 10.1016/j.isci.2020.102012.
[27] A. Tucak *et al.*, “Microneedles: Characteristics, Materials, Production Methods and Commercial Development,” *Micromachines*, vol. 11, no. 11, Art. no. 11, Nov. 2020, doi: 10.3390/mi11110961.
[28] T. Waghule *et al.*, “Microneedles: A smart approach and increasing potential for transdermal drug delivery system,” *Biomed. Pharmacother.*, vol. 109, pp. 1249–1258, Jan. 2019, doi: 10.1016/j.biopha.2018.10.078.
[29] C. O’Mahony, “Structural characterization and in-vivo reliability evaluation of silicon microneedles,” *Biomed. Microdevices*, vol. 16, no. 3, pp. 333–343, Jun. 2014, doi: 10.1007/s10544-014-9836-6.
[30] K. Xu *et al.*, “Efficient decellularization for tissue engineering of the tendon-bone interface with preservation of biomechanics,” *PLoS ONE*, vol. 12, no. 2, p. e0171577, Feb. 2017, doi: 10.1371/journal.pone.0171577.
[31] K. Moussi, A. Bukhamsin, T. Hidalgo, and J. Kosel, “Biocompatible 3D Printed Microneedles for Transdermal, Intradermal, and Percutaneous Applications,” *Adv. Eng. Mater.*, vol. 22, no. 2, p. 1901358, 2020, doi: 10.1002/adem.201901358.
[32] B. Gualeni *et al.*, “Minimally invasive and targeted therapeutic cell delivery to the skin using microneedle devices,” *Br. J. Dermatol.*, vol. 178, no. 3, pp. 731–739, 2018, doi: 10.1111/bjd.15923.
[33] K. Lee *et al.*, “A Patch of Detachable Hybrid Microneedle Depot for Localized Delivery of Mesenchymal Stem Cells in Regeneration Therapy,” *Adv. Funct. Mater.*, vol. 30, no. 23, p. 2000086, 2020, doi: 10.1002/adfm.202000086.
[34] A. H. Morris, J. Chang, and T. R. Kyriakides, “Inadequate Processing of Decellularized Dermal Matrix Reduces Cell Viability In Vitro and Increases Apoptosis and Acute Inflammation In Vivo,” *BioResearch Open Access*, vol. 5, no. 1, pp. 177–187, Jul. 2016, doi: 10.1089/biores.2016.0021.
[35] T. L. Riss *et al.*, *Cell Viability Assays*. Eli Lilly & Company and the National Center for Advancing Translational Sciences, 2016. Accessed: Oct. 07, 2021. [Online]. Available: https://www.ncbi.nlm.nih.gov/books/NBK144065/
[36] “alamarBlue™ Cell Viability Reagent.” https://www.thermofisher.com/order/catalog/product/DAL1025 (accessed Sep. 24, 2021).
[37] “CellTiter-Glo® Luminescent Cell Viability Assay.” https://www.promega.com/products/cell-health-assays/cell-viability-and-cytotoxicity-assays/celltiter_glo-luminescent-cell-viability-assay/ (accessed Sep. 24, 2021).
[38] “LIVE/DEAD™ Viability/Cytotoxicity Kit, for mammalian cells.” https://www.thermofisher.com/order/catalog/product/L3224 (accessed Oct. 08, 2021).

[39] W. Strober, “Trypan Blue Exclusion Test of Cell Viability,” *Curr. Protoc. Immunol.*, vol. 111, p. A3.B.1-A3.B.3, Nov. 2015, doi: 10.1002/0471142735.ima03bs111.
[40] H. A. Alturkistani, F. M. Tashkandi, and Z. M. Mohammedsaleh, “Histological Stains: A Literature Review and Case Study,” *Glob. J. Health Sci.*, vol. 8, no. 3, pp. 72–79, Mar. 2016, doi: 10.5539/gjhs.v8n3p72.
[41] J. Garcia, I. Rios, and F. Fonthal, “Structural and microfluidic analysis of microneedle array for drug delivery,” Aug. 2016, pp. 1–4. doi: 10.1109/SBMicro.2016.7731332.
[42] K. Cheung and D. B. Das, “Microneedles for drug delivery: trends and progress,” *Drug Deliv.*, vol. 23, no. 7, pp. 2338–2354, Sep. 2016, doi: 10.3109/10717544.2014.986309.
[43] H. R. Nejad, A. Sadeqi, G. Kiaee, and S. Sonkusale, “Low-cost and cleanroom-free fabrication of microneedles,” *Microsyst. Nanoeng.*, vol. 4, no. 1, pp. 1–7, Jan. 2018, doi: 10.1038/micronano.2017.73.
[44] K. J. Krieger, N. Bertollo, M. Dangol, J. T. Sheridan, M. M. Lowery, and E. D. O’Cearbhaill, “Simple and customizable method for fabrication of high-aspect ratio microneedle molds using low-cost 3D printing,” *Microsyst. Nanoeng.*, vol. 5, no. 1, pp. 1–14, Sep. 2019, doi: 10.1038/s41378-019-0088-8.
[45] Y.-H. Chen, D.-C. Lin, E. Chern, and Y.-Y. Huang, “The use of micro-needle arrays to deliver cells for cellular therapies,” *Biomed. Microdevices*, Sep. 2020.
[46] K. D. Vernon-Parry, “Scanning electron microscopy: an introduction,” *III-Vs Rev.*, vol. 13, no. 4, pp. 40–44, Jul. 2000, doi: 10.1016/S0961-1290(00)80006-X.
[47] C. M. F. C. Miranda *et al.*, “Effects of chemical and physical methods on decellularization of murine skeletal muscles,” *An. Acad. Bras. Cienc.*, vol. 93, no. 2, p. e20190942, 2021, doi: 10.1590/0001-3765202120190942.
[48] J. Yang, X. Liu, Y. Fu, and Y. Song, “Recent advances of microneedles for biomedical applications: drug delivery and beyond,” *Acta Pharm. Sin. B*, vol. 9, no. 3, pp. 469–483, May 2019, doi: 10.1016/j.apsb.2019.03.007.
[49] “Dr. Pen M8 Microneedling Pen,” *Dr Pen US*. https://us.drpen.co/products/dr-pen-m8 (accessed Aug. 29, 2021).
[50] “ORA Face Microneedle Dermal Roller System 0.5mm - Purple/Black (1 piece) - Dermstore.” https://www.dermstore.com/beauty-ora-facial-microneedle-roller-system-purple-head-with-black-handle-0.5mm/12085479.html?utm_source=googleprod&utm_medium=gp&utm_campaign=gp_bodycare&affil=thggps&switchcurrency=USD&shippingcountry=US&utm_egbu=Dermstore-US_Google-Shopping_Dermstore_Multi_CONV_SSC-DTM-tROAS&utm_egb=Multi&utm_ega=CONV&utm_egc=Dermstore+-+SSC&gclid=CjwKCAjw4KyJBhAbEiwAaAQbE5Z_FG5hOpi0Vk8wyidRedW9tunR2ZMtcBufQG1AxyEFf1IEP45Q1hoC-rcQAvD_BwE&gclsrc=aw.ds (accessed Aug. 29, 2021).
[51] J. Birchall, S. Coulman, D. Shah, and G. Benedetta, “Microneedle Based Cell Delivery,” US 10 232 159 B2, Mar. 19, 2019 [Online]. Available: https://patentimages.storage.googleapis.com/19/f7/da/755f7bae2fb39f/US10232159.pdf
[52] “Zosano Pharma | Transdermal Drug Delivery | Migraine.” https://www.zosanopharma.com/technology/ (accessed Sep. 05, 2021).
[53] “Corium Inc. – Delivering Innovative Transdermal Solutions.” https://www.corium.com/propietary-platforms.html (accessed Sep. 05, 2021).
[54] “BD Micro-Fine Ultra 4mm.” https://www.bd.com/en-uk/products/diabetes/diabetes-products/pen-needles/microfine-4mm-pen-needle (accessed Sep. 05, 2021).
[55] “Product - NanoPass Technologies Ltd.” https://nanopass.com/product/ (accessed Sep. 06, 2021).
[56] “ISO 10993-5:2009 Biological Evaluation of Medical Devices. Part 5: Tests for In Vitro Cytotoxicity.” International Organization for Standardization, 2009.

[57] C. for D. and R. Health, "Use of International Standard ISO 10993-1, 'Biological evaluation of medical devices - Part 1: Evaluation and testing within a risk management process,'" *U.S. Food and Drug Administration*, Sep. 30, 2020. https://www.fda.gov/regulatory-information/search-fda-guidance-documents/use-international-standard-iso-10993-1-biological-evaluation-medical-devices-part-1-evaluation-and (accessed Oct. 13, 2021).
[58] F04 Committee, "Standard Guide for Assessing Medical Device Cytocompatibility with Delivered Cellular Therapies," ASTM International. doi: 10.1520/F3206-17.
[59] F04 Committee, "Guide for Characterization and Testing of Biomaterial Scaffolds Used in Tissue-Engineered Medical Products," ASTM International. doi: 10.1520/F2150-19.
[60] F04 Committee, "Guide for Quantifying Cell Viability within Biomaterial Scaffolds," ASTM International. doi: 10.1520/F2739-19.
[61] "ASTM F2603-06(2020)." https://www.techstreet.com/standards/astm-f2603-06-2020?product_id=2187252 (accessed Oct. 13, 2021).
[62] "ASTM F2952-14." https://www.techstreet.com/standards/astm-f2952-14?product_id=1876797 (accessed Oct. 13, 2021).
[63] 14:00-17:00, "ISO 80369-7:2021," *ISO*. https://www.iso.org/cms/render/live/en/sites/isoorg/contents/data/standard/07/91/79173.html (accessed Jan. 19, 2022).
[64] C. Jiang, C. Cui, L. Li, and Y. Shao, "The Anomalous Diffusion of a Tumor Invading with Different Surrounding Tissues," *PLOS ONE*, vol. 9, no. 10, p. e109784, Oct. 2014, doi: 10.1371/journal.pone.0109784.
[65] "Professional 3D Printing Materials for Digital Dentistry," *Formlabs*. https://dental.formlabs.com/materials/ (accessed Dec. 14, 2021).
[66] "Resin Family: Tough and Durable," *Formlabs*. https://formlabs.com/materials/tough-durable/ (accessed Dec. 14, 2021).
[67] "Detergents for Cell Lysis and Protein Extraction - US." //www.thermofisher.com/us/en/home/life-science/protein-biology/protein-biology-learning-center/protein-biology-resource-library/pierce-protein-methods/detergents-cell-lysis-protein-extraction.html (accessed Dec. 15, 2021).
[68] "Why is EDTA used in lysis buffer? | AAT Bioquest." https://www.aatbio.com/resources/faq-frequently-asked-questions/Why-is-EDTA-used-in-lysis-buffer (accessed Dec. 15, 2021).
[69] C. Segnani *et al.*, "Histochemical Detection of Collagen Fibers by Sirius Red/Fast Green Is More Sensitive than van Gieson or Sirius Red Alone in Normal and Inflamed Rat Colon," *PLoS ONE*, vol. 10, no. 12, p. e0144630, Dec. 2015, doi: 10.1371/journal.pone.0144630.
[70] A. Campos Marín, M. Brunelli, and D. Lacroix, "Flow perfusion rate modulates cell deposition onto scaffold substrate during cell seeding," *Biomech. Model. Mechanobiol.*, vol. 17, no. 3, pp. 675–687, 2018, doi: 10.1007/s10237-017-0985-4.

Glossary

Term	Definition
Autograft	A transplant of tissue from one spot to another from the same individual
Allograft	A transplant of tissue from one individual to another in the same species
BrdU assay	Bromodeoxyuridine assay
Coagulation	Process of liquid (usually blood) changing to a semi-solid/solid state
CNC	Computer Numerical Control Machining
Epidermis	Outer layer of the skin
Ex vivo	Tissue from living organisms tested outside of the body
Extracellular matrix (ECM)	3D structure providing structure and chemical signals to cells
GFP	Green fluorescent protein
Hemostasis	The stopping of blood flow
H & E stain	Hematoxylin and Eosin stain
Immunogenicity	The ability to create an immune response
In vitro	Testing performed outside of a living organism
In vivo	Testing within living organisms
Ischemia	Inadequate blood supply
SEM	Scanning electron microscopy
SLA	Stereolithography 3D Printing
Sarcolemma	Sheath enveloping skeletal muscle fibers
VML	Volumetric muscle loss
Xenograft	A transplant of tissue from one individual to another in different species

Appendices

Appendix A: Decellularization

Appendix A.1 Freeze Protocol: 12 Days

*This procedure is performed at room temperature under agitation, except during the freezing process. The solution should be changed 1-2x per day

1. Cut the tissue samples into the following thicknesses in triplicate: 0.5 cm x 0.5 cm, 1 cm x 1 cm, 2 cm x 2 cm
2. Set aside samples of control muscle that will not be decellularized.
3. Agitate muscle tissue in DI water for 2 minutes. *This leads to cell cytolysis, or cell bursting, due to the hypotonic environment created.*
4. Incubate the muscle tissue in 5 mL of 1X PBS + 0.5% penicillin and streptomycin (99.5 mL PBS + 0.5 mL Pen/strep) for 5 minutes 3 times. This rinsing should occur under agitation on a shaker plate set to 160 r/min. *The PBS creates an isotonic environment to prevent further cell death and rinses the samples to prepare for the next steps. The penicillin and streptomycin prevent bacterial contamination of the tissue.*
5. Remove all solution and freeze the samples at -20℃ for 4 days. *This freezing process causes the cell membrane to rupture.*
6. Rinse the samples in 5 mL of 1X PBS for 20 minutes at room temperature. This rinsing should occur under agitation on a shaker plate set to 160 r/min.
7. Agitate muscle tissue in DI water for 2 minutes.
8. Incubate the samples in 5 mL of 1x PBS + 0.5% penicillin and streptomycin for 5 minutes 3 times. This rinsing should occur under agitation on a shaker plate set to 160 r/min.
9. Incubate the samples in 10 mL of 5 mM EDTA + 50 mM Tris for 2 days (1 mL EDTA + 5 mL Tris + 94 mL DI water). Change solution morning and night. Agitate overnight using a shaker plate set to 100 r/min. *Tris increases the permeability of the cell wall and EDTA is a chelating agent (removes metal ions) that deactivates enzymes and prevents DNA or RNA degradation. Together, Tris and EDTA solubilize DNA and RNA while preventing its degradation.*
10. Rinse the samples with 5 mL of 1X PBS + 0.5% penicillin and streptomycin for 5 minutes 3 times. This rinsing should occur under agitation on a shaker plate set to 160 r/min.
11. Incubate the samples in 10 mL of 1% SDS for 4 days. Change solution morning and night. Agitate overnight using a shaker plate set to 100 r/min.
12. Incubate in 10 mL of 1% Triton X-100 for 2 days (10 mL Triton X-100 + 90 mL DI water). Change solution morning and night. Agitate overnight using a shaker plate set to 100 r/min. *Triton X-100 is a detergent that lyses cells to extract protein and cell organelles. Prolonged exposure to Triton X-100 leads to cell death.*
13. Samples rinsed in 5 mL of 1x PBS + 0.5% antibiotics (3x for 20 min each). This rinsing should occur under agitation on a shaker plate set to 160 r/min.

14. Samples sterilized in 5 mL of 70% alcohol (3x of 30 minutes each). This rinsing should occur under agitation on a shaker plate set to 160 r/min.
15. Samples rinsed in 5 mL of 1X PBS + 0.5% penicillin and streptomycin (3x of 20 min each). This rinsing should occur under agitation on a shaker plate set to 160 r/min.

Appendix A.2 EDTA + Tris Protocol: 9 Days

*****This procedure occurs at room temperature under agitation. The solution should be changed 1-2x per day.

1. Cut the tissue samples into the following thicknesses in triplicate: 0.5 cm x 0.5 cm, 1 cm x 1 cm, 2 cm x 2 cm
2. Set aside samples of control muscle that will not be decellularized.
3. Agitate muscle tissue in DI water for 2 minutes. *This leads to cell cytolysis, or cell bursting, due to the hypotonic environment created.*
4. Incubate the muscle tissue in 5 mL of 1X PBS + 0.5% penicillin and streptomycin (99.5 mL PBS + 0.5 mL Pen/strep) for 5 minutes 3 times. This rinsing should occur under agitation on a shaker plate set to 160 r/min. *The PBS creates an isotonic environment to prevent further cell death and rinses the samples to prepare for the next steps. The penicillin and streptomycin prevent bacterial contamination of the tissue.*
5. Incubate the samples in 10 mL of 5 mM EDTA + 50 mM Tris for 2 days (1 mL EDTA + 5 mL Tris + 94 mL DI water). Change solution morning and night. Agitate overnight using a shaker plate set to 100 r/min. *Tris increases the permeability of the cell wall and EDTA is a chelating agent (removes metal ions) that deactivates enzymes and prevents DNA or RNA degradation. Together, Tris and EDTA solubilize DNA and RNA while preventing its degradation.*
6. Rinse the samples with 5 mL of 1X PBS + 0.5% penicillin and streptomycin for 5 minutes 3 times. This rinsing should occur under agitation on a shaker plate set to 160 r/min.
7. Incubate the samples in 10 mL of 1% SDS for 4 days (5 mL SDS + 95 mL DI water). Change solution morning and night. Agitate overnight using a shaker plate set to 100 r/min. *SDS is an anionic denaturing detergent, which results in disruption of the cell membrane and protein denaturation in the cells.*
8. Incubate the samples with 10 mL of 1X PBS and 1% Triton X-100 for 2 days (10 mL Triton X-100 + 90 mL PBS water). Change solution morning and night. Agitate overnight using a shaker plate set to 100 r/min. *Triton X-100 is a detergent that lyses cells to extract protein and cell organelles. Prolonged exposure to Triton X-100 leads to cell death. In this step the PBS rinses the sample of other detergents*
9. Samples rinsed in 5 mL of 1x PBS + 0.5% antibiotics (3x for 20 min each). This rinsing should occur under agitation on a shaker plate set to 160 r/min.
10. Samples sterilized in 5 mL of 70% alcohol (3x of 30 minutes each). This rinsing should occur under agitation on a shaker plate set to 160 r/min.

11. Samples rinsed in 5 mL of 1X PBS + 0.5% penicillin and streptomycin (3x of 20 min each). This rinsing should occur under agitation on a shaker plate set to 160 r/min.

Appendix A.3 SDS Protocol: 9 Days

*****This procedure occurs at room temperature under agitation. The solution should be changed 1-2x per day.

1. Cut the tissue samples into the following thicknesses in triplicate: 0.5 cm x 0.5 cm, 1 cm x 1 cm, 2 cm x 2 cm
2. Set aside samples of control muscle that will not be decellularized.
3. Agitate muscle tissue in DI water for 2 minutes. *This leads to cell cytolysis, or cell bursting, due to the hypotonic environment created.*
4. Incubate the muscle tissue in 5 mL of 1X PBS + 0.5% penicillin and streptomycin (99.5 mL PBS + 0.5 mL Pen/strep) for 5 minutes 3 times. This rinsing should occur under agitation on a shaker plate set to 160 r/min. *The PBS creates an isotonic environment to prevent further cell death and rinses the samples to prepare for the next steps. The penicillin and streptomycin prevent bacterial contamination of the tissue.*
5. Incubate the samples in 10 mL of 1% SDS for 4 days at room temperature (5 mL SDS + 95 mL DI water). Change solution morning and night. Agitate overnight using a shaker plate set to 100 r/min. *SDS is an anionic denaturing detergent, which results in disruption of the cell membrane and protein denaturation in the cells.*
6. After 4 days, rinse in 5 mL of 1X PBS + 0.5% antibiotics (penicillin and streptomycin) for 5 minutes 3 times. This rinsing should occur under agitation on a shaker plate set to 160 r/min. *The PBS restores the isotonic environment in the sample and rinses away the SDS detergent. The penicillin and streptomycin prevent bacterial growth on the samples.*
7. Incubate the samples in 10 mL of 5 mM EDTA + 50 mM Tris for 2 days (1 mL EDTA + 5 mL Tris + 94 mL DI water). Change solution morning and night. Agitate overnight using a shaker plate set to 100 r/min. *Tris increases the permeability of the cell wall and EDTA is a chelating agent (removes metal ions) that deactivates enzymes and prevents DNA or RNA degradation. Together, Tris and EDTA solubilize DNA and RNA while preventing its degradation.*
8. After 2 days, rinse the samples in 5 mL of 1X PBS + 0.5% penicillin and streptomycin for 5 minutes 3 times. This rinsing should occur under agitation on a shaker plate set to 160 r/min.
9. Incubate the samples in 10 mL of 1% Triton X-100 for 2 days at room temperature (10 mL Triton X-100 + 90 mL DI water). Change solution morning and night. Agitate overnight using a shaker plate set to 100 r/min. *Triton X-100 is a detergent that lyses cells to extract protein and cell organelles. Prolonged exposure to Triton X-100 leads to cell death.*
10. Samples rinsed in 5 mL of 1x PBS + 0.5% antibiotics (3x for 20 min each). This rinsing should occur under agitation on a shaker plate set to 160 r/min.

11. Samples sterilized in 5 mL of 70% alcohol (3x of 30 minutes each). This rinsing should occur under agitation on a shaker plate set to 160 r/min.
12. Samples rinsed in 5 mL of 1X PBS + 0.5% penicillin and streptomycin (3x of 20 min each). This rinsing should occur under agitation on a shaker plate set to 160 r/min.

Appendix B: Histology and Staining Protocols

Appendix B.1 Processing and Embedding Decellularized Tissue Samples

The following protocol was used to process and embed the decellularized tissue samples.

1. The 2 cm samples are too large to fit in cassettes. Cut the 2 cm samples into four pieces longitudinally (along the striations) into equal parts. This will create four 2 cm samples: the outside left, the middle left, the middle right, and the outside right.
2. Place each sample from each size and each decellularization protocol, as well as the control samples, into cassettes and label the cassettes accordingly.
3. Submerge the samples in the cassettes in formalin for at least 24 hours and no longer than 7 days.
4. After the samples have been fixed in formalin, rinse the samples in the cassettes in running water for 5 minutes.
5. Then, load the samples in the cassettes into the Tissue-Tek VIP 6 AI to process the samples. Select the "Routine" protocol, which is a 9 hour protocol.
6. After the samples have been processed, remove the cassettes and drain the machine.
7. Then, use the Leica EG1160 to embed the samples.
    a. Place the samples in the cassettes in the cassette bath.
    b. Then, remove the samples from the cassettes and place them into the metal molds.
    c. Use the Paraffin dispenser to dispense paraffin over the sample.
    d. Place the cassette bottom on top of the sample in the mold and add paraffin to fill the mold and cassette bottom ¾ of the way full.
    e. Place on the cold plate for 30 minutes to allow the samples to solidify.

Appendix B.2 Microtoming Decellularized Tissue Samples

The following protocol was used to section the decellularized tissue samples prior to staining using the Leica RM2235 Microtome.

1. Prepare the water bath so that the water temperature reaches 44℃.
2. Prepare a bucket of ice and place the specimen blocks into the ice bucket prior to sectioning.
3. Ensure the handwheel on the right side of the machine is upright and locked.
4. Set the desired section thickness with the dial knob on the front face to 5 μm.
5. If a blade is already in the knife holder, cover the blade with the red blade guard and flip the clamping lever to retract the knife blade holder away from the cassette clamp.
6. Pinch the top bar of the cassette clamp to lower the bottom bar and place the specimen block in the clamp with the beveled edge of the cassette towards the right hand side, then release the top bar of the clamp to secure the block.
7. Reposition the knife holder base in front of the specimen block and secure the sloping lever on the bottom right edge.
8. If the blade needs to be changed, flip the lever to the left of the blade and release the knife clamp. Remove the blade carefully with forceps and discard in the sharps container.

9. Place the fresh blade in the slot using forceps. Flip the left-slide lever to clamp the new blade into place.
10. If needed, flip the lever on the right side of the knife holder to reposition the blade laterally. Once the blade is positioned correctly, secure the lever again.
11. Ensure that all clamping levers are secured before operating the microtome.
12. Flip the red blade guard down to expose the blade.
13. Turn the small coarse feed wheel on the left side of the microtome to position the blade in front of the specimen block.
14. Unlock the handwheel on the right side and turn it clockwise (forward) to begin trimming the block.
15. To expose the specimen within the block, press the mechanical trimming lever on the left side of the front face and turn the right-side handwheel to trim the block coarsely. The lever has two settings that determine the thickness of the coarse trim: 10 μm and 30 μm. Once the specimen is exposed, release the trimming lever.
16. Begin sectioning by turning the right-side handwheel.
17. Sections will slide down the blade in a thin ribbon. Once a ribbon reaches the desired length, gently remove it from the blade with forceps or another tool and carefully float it in the water bath.
18. If paraffin begins to build up on the blade, brush it away with a paintbrush or a wadded up Kimwipe™. Do not touch the blade directly.
19. If the sections show artifacts even though the blade is clean, repeat step 8 to position a fresh portion of the blade in front of the specimen block.
20. When finished with a block and need to start a new one, lock the right-side handwheel and repeat steps 3-5. Never change the block with the blade unguarded and positioned in front of the cassette clamp.
21. When finished with the microtome, remove and discard the blade as in step 6. Use a paintbrush to remove any paraffin or other debris from the microtome and throw it away. The waste tray underneath the knife holder block can be removed for easier cleaning.
22. Return all components of the microtome to their original positions. Wipe down levers and handwheels with 70% ethanol. When finished with the water bath, dump out the water and remove any paraffin residues. If need be, bring the water bath to a fume hood and clean with gauze dipped in xylene. Leave the water bath to dry in the fume hood.

Appendix B.3 Hematoxylin and Eosin (H&E) Staining Protocol

The following protocol was used to carry out the hematoxylin and eosin (H&E) staining of sections of our decellularized tissue samples.

1. Bake the slides in the warming oven for 30 minutes prior to staining.
2. Submerge the slides in xylene I for 3 minutes.
3. Submerge the slides in xylene II for 3 minutes.
4. Submerge the slides in xylene III for 3 minutes.

5. Submerge the slides in 100% EtOH I for 3 minutes.
6. Submerge the slides in 100% EtOH II for 3 minutes.
7. Submerge the slides in 95% EtOH for 1 minute.
8. Submerge the slides in75% EtOH for 1 minute.
9. Rinse the slides in running water for 5 minutes, ensuring that the water is not directly pouring onto the surface of the slides.
10. Filter Harris Hematoxylin into the soaking container using a coffee filter.
11. Submerge the slides in Harris Hematoxylin for 5 minutes
12. Rinse the slides in running water until the water runs clear. While this occurs, use a coffee filter to filter the Harris Hematoxylin back into the stock solution bottle.
13. Differentiate the slides in acid alcohol by dipping the slides in with 3 quick dips.
14. Rinse the slides in running water for 30 seconds.
15. Submerge the slides in ammonia water for 1 minute.
16. Rinse the slides in warm running water for 5 minutes.
17. Submerge the slides in 95% EtOH for 1 minute.
18. Counterstain the slides using Eosin Y by submerging the slides in the stain for 1 minute.
19. Submerge the slides in 95% EtOH I for 30 seconds.
20. Submerge the slides in 95% EtOH II for 30 seconds.
21. Submerge the slides in 100% EtOH III for 1 minute.
22. Submerge the slides in 100% EtOH IV for 1 minute.
23. Submerge the slides in xylene IV for 1 minute.
24. Submerge the slides in xylene V for 1 minute.
25. Submerge the slides in xylene VI until immediately ready to mount coverslips onto the slides.
26. Mount the slides onto the coverslips using Cytoseal 60 from Thermo Scientific. Ensure that no bubbles are trapped between the coverslips and the slides.
27. Image the slides using an Iphone camera and a VistaVision upright microscope.

Appendix B.4 Picrosirius Red/Fast Green Staining Protocol

The following protocol was used to carry out the picrosirius red/fast green staining of sections of our decellularized tissue samples.

1. Bake the slides in the warming oven for 30 minutes prior to staining.
2. Submerge the samples in xylene I for 3 minutes.
3. Submerge the samples in xylene II for 3 minutes.
4. Submerge the samples in xylene III for 3 minutes.
5. Submerge the samples in 100% EtOH I for 3 minutes.
6. Submerge the samples in 100% EtOH II for 3 minutes.
7. Submerge the samples in 90% EtOH for 1 minute.
8. Submerge the samples in 75% EtOH for 1 minute.

9. Rinse the slides in running water for 5 minutes, ensuring that the water is not directly pouring onto the surface of the slides.
10. Submerge the slides in picrosirius red/fast green stain for 30 minutes.
11. Submerge the slides in 80% EtOH for 1 minute.
12. Submerge the slides in 95% EtOH I for 1 minute
13. Submerge the slides in 95% EtOH II for 30 seconds.
14. Submerge the slides in 100% EtOH III for 1 minute.
15. Submerge the slides in 100% EtOH IV for 1 minute.
16. Submerge the slides in 100% EtOH V for 1 minute.
17. Submerge the slides in xylene IV for 1 minute.
18. Submerge the slides in xylene V for 1 minute.
19. Submerge the slides in xylene VI for 1 minute.

Appendix C: Testing Protocols

Appendix C.1 Cellular Viability Testing Protocol

*To be completed in a sterile biosafety cabinet

1. Prepare the hood with three 15 mL conical tubes. One tube should contain isopropyl alcohol and the other two tubes should contain 1X DPBS (positive or negative). To sterilize the forceps, dip them into the isopropyl alcohol for 5-10 minutes, then dip them into the first DPBS tube and then dip them into the third DPBS tube.
2. Remove decellularized tissue blocks from the conical tubes using sterile forceps. Cut the tissue blocks into slices and place in the bottom of a well plate or tissue culture dish. Prepare three tissue slices for each cell density being tested.
3. Perform subculture on cells, counting cells and resuspending at a concentration of 10 million cells per mL.
4. Perform the following serial dilution:

Table C.1 Serial Dilution was conducted using these volumes and cell densities.

Medium (uL)	NA	250 uL	250 uL	250 uL
Cell Suspension (uL)	1000	250 uL	250 uL	250 uL
Cell density (per uL)	10,000	5,000	2,500	1,000

5. Seed the cells on each tissue slice in 20-30 uL drops at a cell density of 10000 cells/uL (10 million cells/mL), 5000 cells/uL (5 million cells/mL), 2500 cells/uL (2.5 million cells/mL), 1000 cells/uL (1 million cells/mL).
6. Pipette 20 uL onto the center of the tissue pieces as a droplet. Add 1 mL of medium to the neighboring wells that do not contain tissue samples. This media will prevent evaporation. Allow the cells to attach at room temperature for 3 hours in an incubator at 37°C and 5% CO_2.
7. After the cells have attached, add media to the wells to bring up the total media to 1 mL (submerge the decellularized bovine skeletal muscle pieces) and incubate at 37°C and 5% CO_2 for 7 days. Image the tissue slices with cells on days 3 and 7.

Appendix C.2 Long-term Freezing Testing Protocol

1. Mark two 15 mL conical tubes as Freezing solution A and Freezing solution B
    a. Freezing solution A will contain complete media (5 mL)
    b. Freezing solution B will contain 4 mL of CM and 1 mL of 20% DMSO
2. Transfer 1 mL of media into a tube with the decellularized tissue sample.
3. Slowly introduce 1 mL of freezing solution B into the tube with the decellularized tissue and media.

4. Transfer the tubes to the CoolCell Freezing containers in the -20℃ freezer. Transfer six of the nine samples to the -80℃ freezer the next day. After 24 hours, transfer three samples from the -80℃ freezer to liquid nitrogen.
5. After more than 1 week, thaw the cryovials from each of the storage conditions and remove the decellularized tissue slices. Place these tissue slices in a 24 well plate.
6. Perform subculture on cells, counting cells and resuspending at a volume of 10 million cells per mL.
7. Seed the cells on each tissue slice in 20-30 uL drops at a cell density of 10000 cells/uL (10 million cells/mL).
8. Pipette 20 uL onto the center of the tissue pieces as a droplet. Add 1 mL of medium to the neighboring wells that do not contain tissue samples. This media will prevent evaporation. Allow the cells to attach at room temperature for 3 hours in an incubator at 37℃ and 5% CO_2.
9. After the cells have attached, add media to the wells to bring up the total media to 1 mL (submerge the decellularized bovine skeletal muscle pieces) and incubate at 37℃ and 5% CO_2 for 7 days. Image the tissue slices with cells on days 3 and 7.

Appendix C.3 SEM Sample Preparation and Imaging Protocol

The following protocol was used to prepare and image control and decellularized tissue samples using SEM. Imaging was conducted on the Phenom G1 Scanning Electron Microscope.

1. Fix samples in neutral buffered formalin for 2 hours at room temperature.
2. Incubate samples in 1X PBS three times for 5 minutes each rinse.
3. Incubate samples in 50% EtOH for 15 minutes.
4. Incubate samples in 70% EtOH for 15 minutes.
5. Incubate samples in 90% EtOH for 15 minutes.
6. Incubate samples in 100% EtOH for 15 minutes.
7. Incubate samples in 100% EtOH for 15 minutes.
8. Incubate samples in a 1:2 solution of HDMS:100% EtOH for 20 minutes.
9. Incubate samples in a 2:1 solution of HDMS: 100% EtOH for 20 minutes
10. Incubate samples in 100% HDMS for 20 minutes.
11. Incubate samples in 100% HDMS overnight to dry the samples.
12. Ensure samples are no larger than 25 mm in diameter and 30 mm in height.
13. Attach the samples to the SEM sample stage and dry each sample with compressed air 6-12 inches away.
14. Using gloves and tweezers, load the sample mount onto the sample holder. Start with the sample flush with the top of the sample holder, and move it down four notches (~2 mm).
15. Fully open the sample loading door and insert the sample holder.
16. Ensure that the sample indicator light is green when the sample is orange.
17. Focus the optical image with the mouse wheel on the computer monitor and build a composite optical image for the sample.
18. Click the “two plus (+)” icon to switch the monitor view to SEM.

19. Click the single plus sign icon and use the mouse to increase or decrease magnifications.
20. Click the camera icon to snap an image of the sample.
21. Click archive to view the captured images.
22. Image parameters can be adjusted in settings, including setting the image to compositional or topographical.
23. Use the eject button to remove the sample holder from the machine and finish the imaging session.
24. Upload each image into ImageJ.
25. Remove the previous scale by selecting Analyze > Set Scale.
26. Draw a line with the line tool over the image's scale bar.
27. Select Analyze > Set Scale and enter the known distance and units.
28. Apply a bandpass filter by selecting Process > FFT > Bandpass filter.
29. Select Image > Adjust > Threshold and select the red threshold option.
30. Adjust the top bar so that the red filter covers all or a majority of pores without including too much feedback.
31. Click Apply.
32. Select Analyze > Analyze Particles > Show outlines, display results.
33. Save the data as an Excel file, then use the MAX and MIN function on Excel to determine the minimum and maximum pore area of each image to find the smallest pore among the samples and the largest pore among the samples.

Appendix C.4 Leak Testing Protocol

The following protocol was used to ensure that there was no leakage in our device design.

1. Device is assembled and air is loaded into the syringe.
2. Deionized water is poured into a 50mL beaker until the device can fully submerge.
3. Device is submerged sideways into the beaker and gas release is observed as the air is pushed out of the syringe.

Appendix C.5 Volume and Cell Retention Testing Protocol

The following protocol was used to determine the retention of cells after delivery within decellularized tissue scaffolds using our microneedle device.

1. Weigh the tissue before delivery of cell suspension.
2. Place each tissue sample in a separate well in a 12-well plate.
3. Deliver 250 uL of cell suspension at a concentration of 10 million cells/mL to the decellularized tissue samples.
4. Take the tissue out of the dish, lightly dab away any fluid on the outside, and weigh the tissue. Note if there is a change in weight after delivery of cells and media.
5. After taking the tissue out, pipette the cell suspension remaining in the dish and count the cells to determine the number of cells that did not attach to the tissue.

Appendix C.6 Flow-Rate and Cell Delivery Testing Protocol

The following protocol was used to determine the optimal flow rate to deliver cells to decellularized tissue samples and determine if cells remained in the samples.

1. Incubate nine decellularized tissue scaffolds in complete media (10% FBS) overnight.
2. Remove the scaffolds from the media and place them in a 12-well plate.
3. Perform cell subculture, counting cells and resuspending at 1 million cells/mL.
4. Collect 5 mL of cell suspension in a 5 mL BD syringe.
5. Assemble the syringe pump microneedle reservoir system as follows:
    a. Attach a 25 gauge blunt end needle adaptor to the end of the syringe and one to the top of the microneedle reservoir.
    b. Attach 0.86 mm inner diameter polyethylene tubing (Intramedic PE90 427421) to both adaptors to connect the syringe and the microneedle reservoir.
    c. Secure the syringe in the syringe pump system.
    d. Set the diameter on the syringe pump to 12.07 mm (the inner diameter of a 5 mL BD syringe).
6. Set the first flow-rate to 0.6 mL/min and press start.
7. Allow the tubing and microneedle reservoir to fill with media until cell suspension starts dripping out of the needles.
8. After cell suspension has started dripping out, insert the needles into the tissue scaffold about halfway and allow 1 mL of cell suspension to be delivered to the scaffold.
9. Stop the pump and move to the next scaffold. Then press start.
10. Repeat steps 8 and 9 for the third scaffold.
11. After three samples have had cell suspension delivered at 0.6 mL/min, remove the 25 gauge blunt end needle adaptors and the tubing.
12. Take up 5 mL in the syringe again and assemble the system as in step 5.
13. Set the flow rate to 1.2 mL/min and press start.
14. Repeat steps 7-11.
15. Take up 5 mL in the syringe again and assemble as described in step 5.
16. Set the flow rate to 1.8 mL/min and press start.
17. Pipette the suspension that leaked out of the scaffolds out of the wells and count the cells in the suspension for each flow rate to determine the number of cells that were retained by the scaffold.
18. Add 2 mL of media to each well and return the wells with the scaffolds to the incubator for 3 days.
19. After 3 days, perform histology and H&E staining as described in Appendix B to determine if cells remain in the scaffolds.

Appendix D: Histology and H&E Staining for Protocol Optimization

The following figures show the results from the H&E staining of decellularized chicken samples after decellularization with three different protocols. Three sets of samples, A, B, and C, were performed for each decellularization protocol, sectioned using a microtome, and stained. The image of the 0.5 cm sections from sample C of the SDS protocol was too small to put onto a slide and was therefore not imaged.

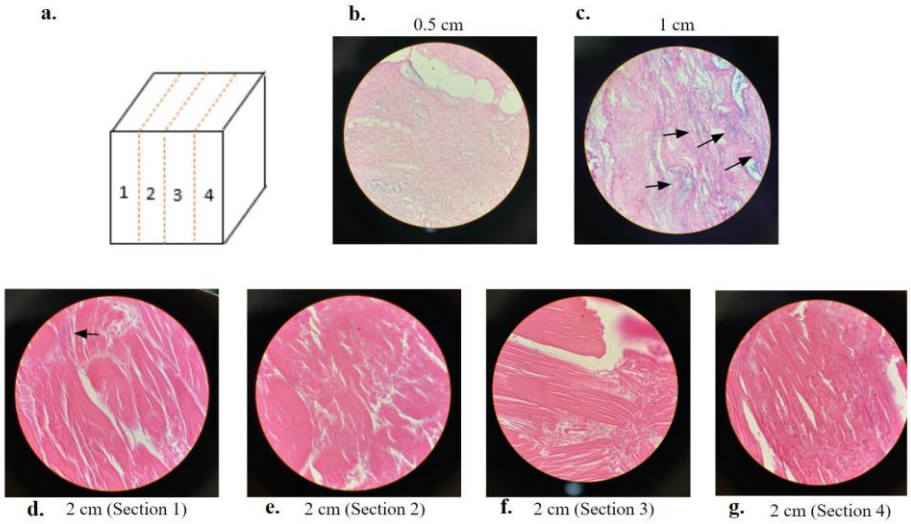

Figure D.1 H&E Staining of Decellularized Samples from Freeze Protocol Sample B. Images were selected from one of three sets of samples as representative results (Sample B). The 2cm^3 control samples were sectioned (a) and stained in four parts (d-g). The 0.5cm^3 (b) and the 1cm^3 (c) samples were stained as a whole piece. Pink stain represents cytoplasm and purple stain represents cell nuclei. Black arrows indicate cells.

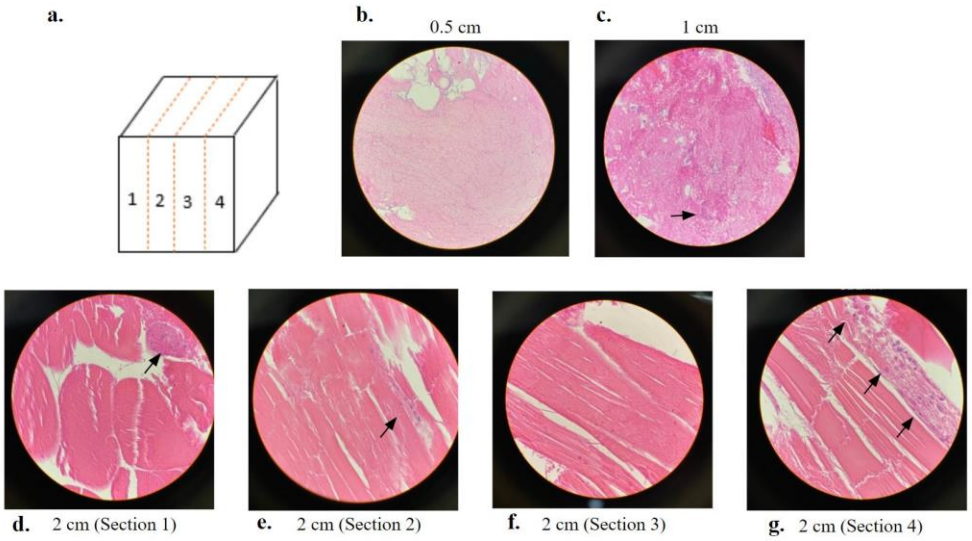

Figure D.2 H&E Staining of Decellularized Samples from EDTA + Tris Protocol Sample B. Images were selected from one of three sets of samples as representative results (Sample B). The 2cm^3 control samples were sectioned (a) and stained in four parts (d-g). The 0.5cm^3 (b) and the 1cm^3 (c) samples were stained as a whole piece. Pink stain represents cytoplasm and purple stain represents cell nuclei. Black arrows indicate cells.

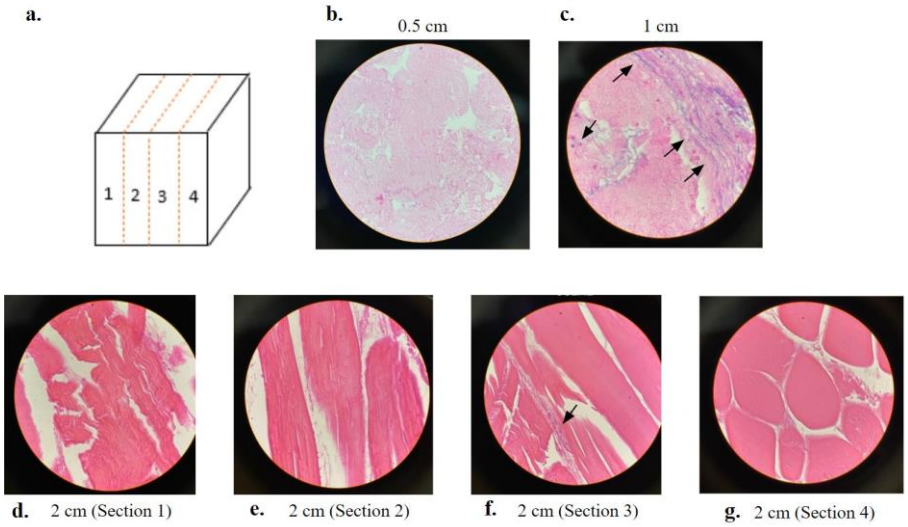

Figure D.3 H&E Staining of Decellularized Samples from EDTA + Tris Protocol Sample C. Images were selected from one of three sets of samples as representative results (Sample C). The 2cm^3 control samples were sectioned (a) and stained in four parts (d-g). The 0.5cm^3 (b) and the 1cm^3 (c) samples were stained as a whole piece. Pink stain represents cytoplasm and purple stain represents cell nuclei. Black arrows indicate cells.

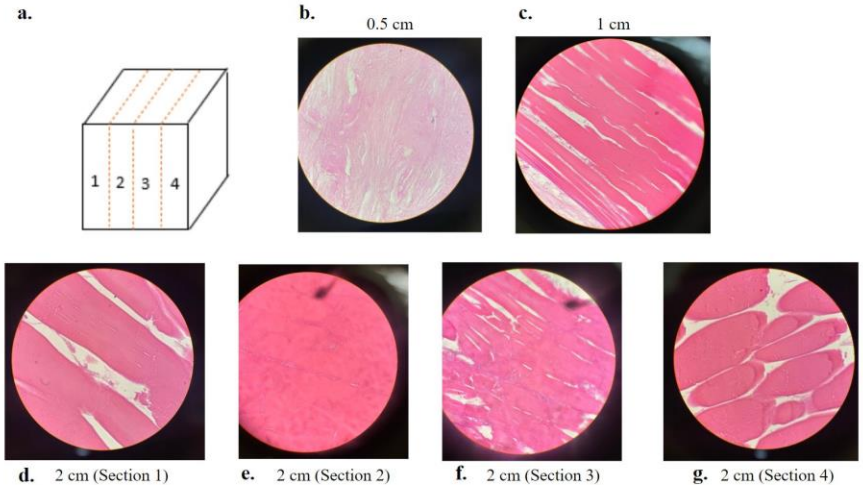

Figure D.4 H&E Staining of Decellularized Samples from SDS Protocol Sample B. Images were selected from one of three sets of samples as representative results (Sample B). The 2cm^3 control samples were sectioned (a) and stained in four parts (d-g). The 0.5cm^3 (b) and the 1cm^3 (c) samples were stained as a whole piece. Pink stain represents cytoplasm and purple stain represents cell nuclei. Black dots are debris on the microscope.

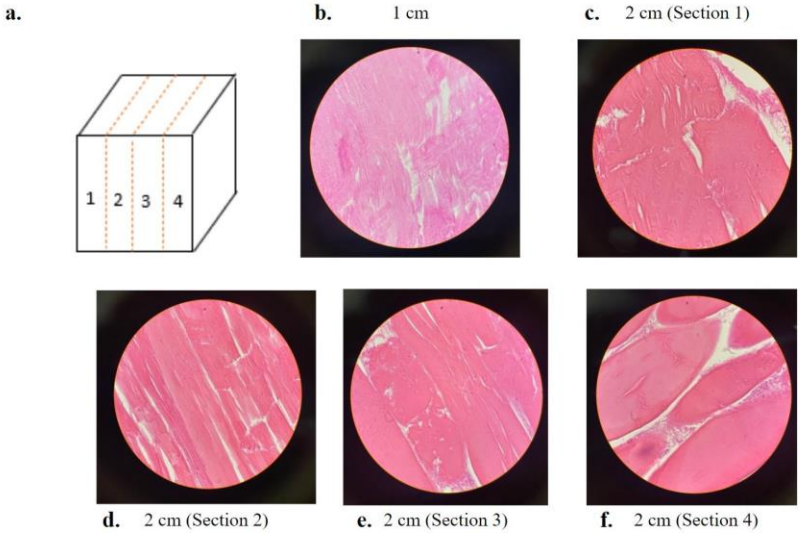

Figure D.5 H&E Staining of Decellularized Samples from SDS Protocol Sample C. Images were selected from one of three sets of samples as representative results (Sample C). The 2cm^3 control samples were sectioned (a) and stained in four parts (d-g). The 0.5cm^3 (b) and the 1cm^3 (c) samples were stained as a whole piece. Pink stain represents cytoplasm and purple stain represents cell nuclei.

Appendix E: Flow Rate and Cell Delivery Testing

The following figures show the results from the H&E staining of decellularized bovine skeletal muscle after cells were delivered at three flow rates: 0.6 mL/min, 1.2 mL/min, and 1.8 mL/min.

Figure E.1 H&E Staining of Decellularized and Recellularized Bovine Skeletal Muscle at 0.6 mL/min Flow Rate. Images were selected from the center of the 1 cm thick muscle tissue. Pink stain represents cytoplasm and purple stain represents cell nuclei. Black circles = nuclei.

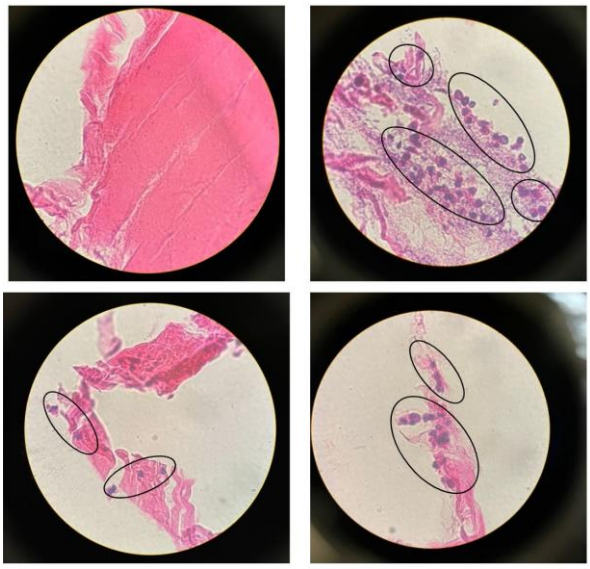

Figure E.2 H&E Staining of Decellularized and Recellularized Bovine Skeletal Muscle at 1.2 mL/min Flow Rate. Images were selected from the center of the 1 cm thick muscle tissue. Pink stain represents cytoplasm and purple stain represents cell nuclei. Black circles = nuclei.

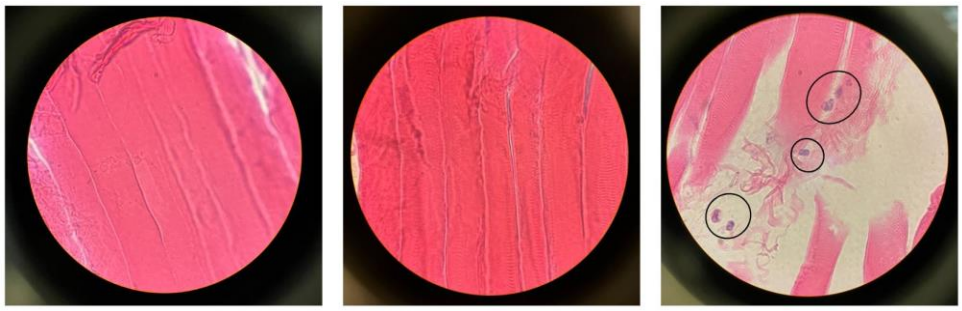

Figure E.3 H&E Staining of Decellularized and Recellularized Bovine Skeletal Muscle at 1.8 mL/min Flow Rate. Images were selected from the center of the 1 cm thick muscle tissue. Pink stain represents cytoplasm and purple stain represents cell nuclei. Black circles = nuclei.

Appendix F: SolidWorks Computer Aided Design Drawings

The following figures show the CAD drawings used during device fabrication.

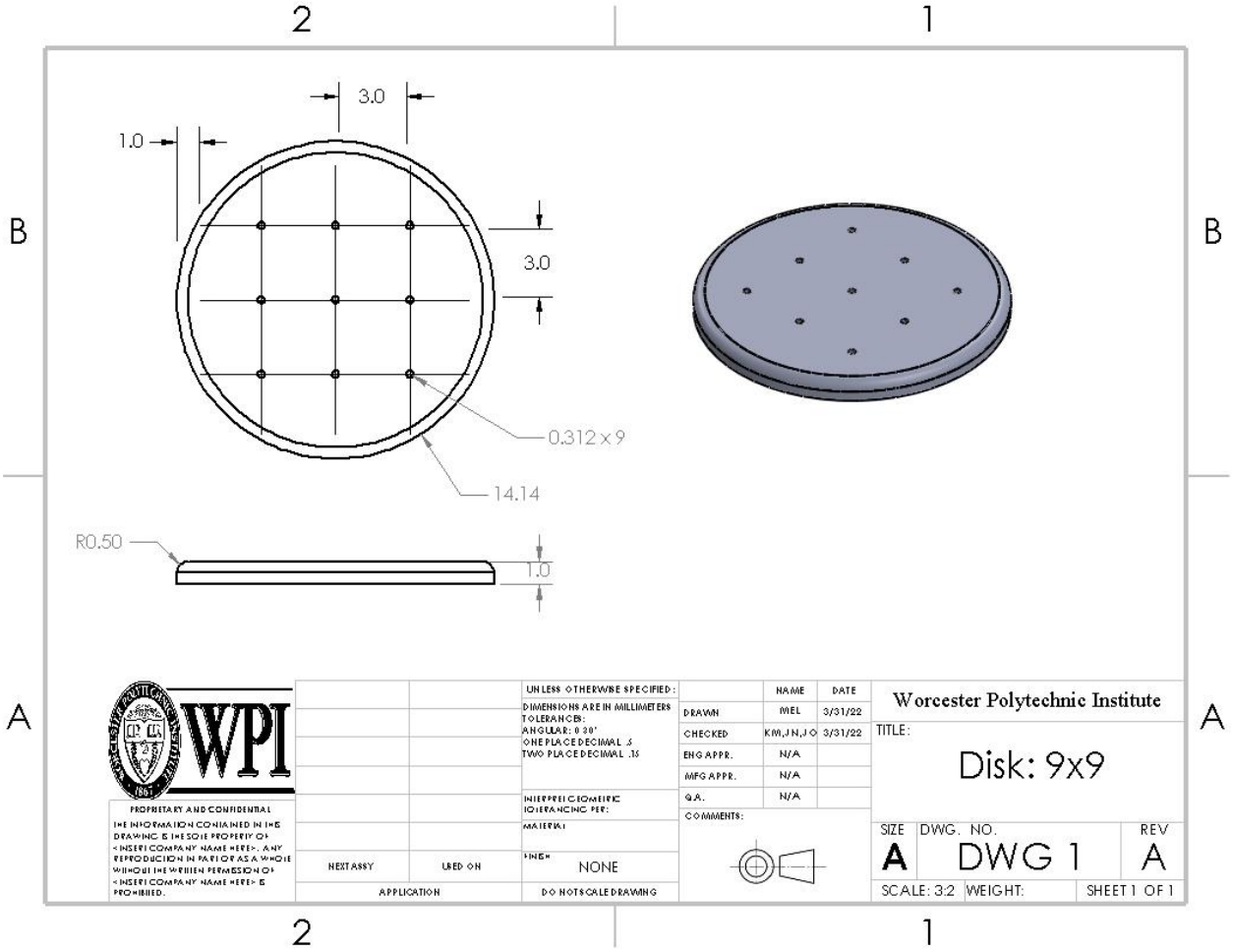

Figure F.1 CAD Drawing of the disk with a 9x9 hole array.

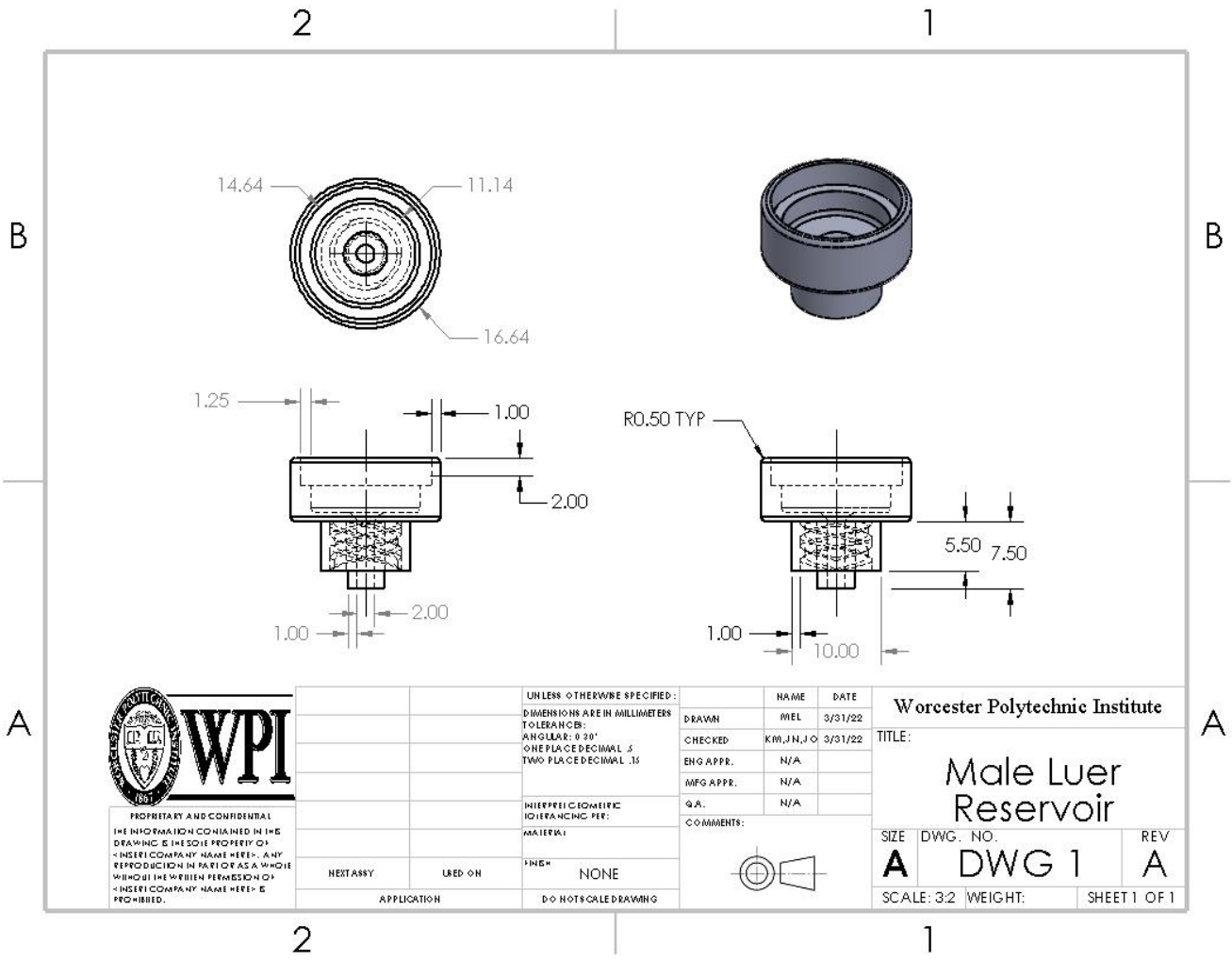

Figure F.2 CAD Drawing of the reservoir.

Appendix G: Gantt Chart

The following table is the Gantt chart the team used to manage and organize their MQP.

Table G.1: Gantt Chart for 2021-2022 Year. Each task shows the expected time period to complete the task with blue highlighted boxes.

Task	**Summer 2021**							
Begin Literature Review								
	A-Term							
	8/22-8/28	8/29-9/4	9/5-9/11	9/12-9/18	9/19-9/25	9/26-10/2	10/3-10/9	10/10-10/16
Literature Review								
Determine Design Objectives/ Constraints								
Brainstorm Designs								
Pugh Analysis								
Brainstorm Potential Validation and Verification Methods								
Determine Potential Stakeholders								
Decellularizatio n Protocol Optimization								
	B-Term							
	10/24-10/30	10/31-11/6	11/7-11/13	11/14-11/20	11/21-11/27	11/28-12/4	12/5-12/11	12/12-12/18
Model Final Design in SolidWorks								
Perform Decellularizatio								

n for Protocol Optimization								
Process Samples in Histology Core								
Microtome Samples								
Staining and Imaging Samples								
Determine Optimal Decellularizatio n Protocol								
Iterative Prototyping of Final Design								
3D Printing of Design Pieces								
	C-Term							
	1/9-1/15	1/16-1/22	1/23-1/29	1/30-2/5	2/6-2/12	2/13-2/19	2/20-2/26	2/27-3/5
CNC Drilling of Parts								
Press Fitting and Epoxying Needles								
Decellularizatio n of Bovine Muscle								
Processing Samples in Histology Core								
Microtoming Samples								
Collagen Staining and Imaging of Histological Sections								
H&E Staining								

and Imaging of Histological Sections								
SEM Sample Prep and Imaging								
Cell Viability Testing								
Volume and Cell Retention Testing								
Viscosity Testing								
Device Leak Test								
Long-Term Storage of Decellularized Tissue								
	D-Term							
	3/13-3/19	3/20-3/26	3/27-4/2	4/3-4/16	4/10-4/16	4/17-4/23	4/24-4/30	5/1-5/3
Decellularization of Bovine Muscle								
Delivery of Cells with Device at different flow rates and H&E Staining								
BrdU Proliferation Assay								
Long-Term Storage of Decellularized Tissue (continued)								
Submit Project Abstract								
Finalize Report								

Complete Presentation								
Project Presentation Day								
Submit eCDR								
Project Clean-up								